Published in final edited form as:

Nature. 2017 December 07; 552(7683): 57–62. doi:10.1038/nature25005.

A tRNA-derived small RNA regulates ribosome biogenesis

Hak Kyun Kim[1,2], **Gabriele Fuchs**[3,6], **Shengchun Wang**[1,2,5], **Wei Wei**[4], **Yue Zhang**[1,2,7], **Hyesuk Park**[1,2], **Biswajoy Roy-Chaudhuri**[1,2,9], **Pan Li**[8], **Jianpeng Xu**[1,2], **Kirk Chu**[1,2], **Feijie Zhang**[1,2], **Mei-Sze Chua**[4], **Samuel So**[4], **Qiangfeng Cliff Zhang**[8], **Peter Sarnow**[3], and **Mark A. Kay**[1,2,*]

[1]Department of Pediatrics, Stanford University, Stanford, CA94305, USA

[2]Department of Genetics, Stanford University, Stanford, CA94305, USA

[3]Department of Microbiology and Immunology, Stanford University, Stanford, CA 94305, USA

[4]Asian Liver Center, Department of Surgery, Stanford University School of Medicine, Stanford, CA 94305, USA

[8]MOE Key Laboratory of Bioinformatics, Beijing Advanced Innovation Center for Structural Biology, Center for Synthetic and Systems Biology, Tsinghua-Peking Joint Center for Life Sciences, School of Life Sciences, Tsinghua University, Beijing 100084, China

Abstract

tRNA-derived small RNAs (tsRNAs; also called tRNA-derived fragments (tRFs)) are an abundant class of small non-coding RNAs whose biological roles are not well defined. We show that inhibition of a specific tsRNA, LeuCAG3′tsRNA, induces apoptosis in rapidly dividing cells *in vitro* and in a patient-derived orthotopic hepatocellular carcinoma model in mice. This tsRNA binds at least two ribosomal protein mRNAs (for RPS28 and RPS15) to enhance their translation. Reduction of RPS28 mRNA translation blocks pre-18S ribosomal RNA processing, resulting in a

*Correspondence and requests for materials should be addressed to M.A.K. (markay@stanford.edu).
[5]Current address: Medtronic Vascular, 3576 Unocal Place, Santa Rosa, CA 95403, USA
[6]Current address: The RNA Institute and Department of Biological Sciences, University at Albany, State University of New York, 1400 Washington Ave., Albany, NY, 12222, USA
[7]Current address: Stanford Center for Genomics and Personalized Medicine, 3165 Porter Drive, Palo Alto, CA94304, USA
[9]Current address: Impossible Foods Inc., 525 Chesapeake Dr., Redwood City, CA94063, USA

Supplementary Information is available in the online version of the paper.

Author Contributions H.K. contributed to experimental design, interpretation, execution, and manuscript writing and editing. G.F. performed experiments in Fig. 3a,b, and Extended Data Fig. 1g,h, and assisted with interpretation, discussion and manuscript editing. S.W. performed experiments in Figs. 1c, 2b and Extended Data Figs. 1i, 2c. W.W. designed experiments with the PDX model and conducted experiments in Fig. 2c and Extended Data Fig. 2h,i,k. Y.Z. performed computational analyses (RNA-seq and predictions of tsRNA binding sites on pre-45S rRNA) in Extended Data Figs. 3d and 5a. H.P. performed multiple experiments including Figs. 2a,d, 4a,e, and 5b. B.R.C. conducted the experiment in Extended Data Fig. 8a. P.L. analyzed icSHAPE data in Extended Data Fig. 9b. J.X. performed LeuCAG3′tsRNA target site prediction in Extended Data Figs. 8b, 9a. F.Z. performed RNA extraction and mouse experiments. K.C. conducted protein extraction. M.C. designed experiments with PDX model, interpreted animal data and assisted in manuscript editing. S.S. recruited the PDX model and provided discussion regarding the xenograft model. Q.C.Z. analyzed, interpreted and discussed icSHAPE data. P.S. interpreted and discussed experimental results and assisted in manuscript editing. M.A.K. contributed to the experimental design, data interpretation, and manuscript writing and editing.

The authors declare no competing financial interests. HK, SW and MAK are inventors on relevant patents filed by Stanford University.

decrease in the number of 40S ribosomal subunits. These data establish another post-transcriptional mechanism that can fine-tune gene expression during different physiological states and provide a potential new target for treating cancer.

tsRNAs are categorized into at least six types based on the cleavage position of the mature or precursor tRNA transcript[1]. Stress-induced 30- to 40-nucleotide (nt) tRNA halves are generated by angiogenin[1–3] and affect cell proliferation, apoptosis, and epigenetic inheritance[4–7]. 5′ tRNA halves also inhibit global translation[8,9]. There is growing evidence that some of the shorter 5′ and 3′ ends of mature tRNA-derived 18- to 22-nt type I tsRNAs (5′ and 3′ tsRNAs), and type II tsRNAs derived from the 3′ end of precursor tRNAs, play important roles in cellular homeostasis[7] and in the regulation of transposition[10,11]; it remains controversial whether they can function as a microRNA (miRNA)[12–14]. Because type I tsRNAs are derived from mature tRNAs, their sequences are more highly conserved between species. During our study of tsRNAs, we uncovered a new functional role for the 22-nt LeuCAG3′tsRNA in regulating ribosome biogenesis.

LeuCAG3′tsRNA is essential for cell viability

We identified and selected tsRNAs from expression screens in HeLa and HCT-116 cells and used locked nucleic acid/DNA-mixed anti-sense oligonucleotides (LNA/ASO mixmer)[15,16] to inhibit various transcripts (Fig. 1a). Blocking the LeuCAG3′tsRNA with a complementary mixmer LNA significantly reduced cell viability as determined by MTS cell proliferation[17] and counting assays (Fig. 1a,b and Extended Data Fig. 1a–d). Various controls (LNAs containing scrambled sequence, 2-nt mismatches, complementarity to other regions of the Leu-tRNA, or directed against other 3′ tsRNAs) did not affect cell viability (Fig. 1a,b and Extended Data Fig. 1a–d). Similar results were obtained using an LNA/DNA gapmer ASO that induces RNase H-mediated cleavage of the target RNA[15] (Extended Data Fig. 1e). These effects were not due to loss of the mature tRNA because there was no LNA binding or degradation of the intact mature LeuCAG-tRNA (Extended Data Fig. 1f), and no significant reduction in global protein synthesis (Extended Data Fig. 1g–i). Finally, we replaced 13 Leu CUG codons with Leu non-CUG (CUC or CUU) codons from the *Renilla* gene and left the firefly luciferase gene unmodified (Supplementary Table 1) in the psicheck2 expression plasmid. Substitution of the Leu codons did not affect *Renilla* luciferase expression in the presence or absence of the LNA (Fig. 1c). Thus, the anti-Leu3′tsLNA did not affect mature LeuCUG-tRNA function.

Standard deep sequencing methods cannot accurately quantify tsRNA species due to abundant post-transcriptional tRNA modifications (Extended Data Fig. 1j)[18,19]. Northern blot analyses demonstrated that the major isoform of the LeuCAG3′tsRNA was 22- and not 18-nt (Extended Data Fig. 1k). In contrast to the effect of tsRNA knockdown, transfection of a synthetic 22-nt LeuCAG3′tsRNA into cells increased cell viability (Fig. 1d). The specificity of this outcome was supported by the lack of a growth response using two different controls, and a 27-nt 3′ end of LeuCAG-tRNA containing an additional 5-nt of LeuCAG-tRNA sequence.

Three different assays[20] established that LeuCAG3′tsRNA-inhibited cells undergo apoptosis. Using Annexin V and PI staining and flow cytometry analysis (Fig. 2a and Extended Data Fig. 2a), we observed that three days after transfection, the percentage of LeuCAG3′tsRNA-inhibited HeLa cells undergoing early and late apoptosis was 21.5±4.6% and 24.5±2.7, respectively, compared to 5.7±1.4% and 4.6±1.2% in control cells (Fig. 2a). Similar results were obtained in HCT-116 cells (Extended Data Fig. 2b). Induction of apoptosis was confirmed in both HeLa and HCT-116 cells by TUNEL staining (Fig. 2b and Extended Data Fig. 2c), and PARP cleavage (Extended Data Fig. 2d,e).

Inhibition of LeuCAG3′tsRNA suppresses tumor growth

Hydrodynamic transfection of 125 μg of anti-Leu3′tsLNA into normal mice to achieve a rapid and high concentration of oligonucleotide in liver hepatocytes did not affect serum ALT levels, a sensitive marker for liver toxicity (Extended Data Fig. 2f). Because we observed the LeuCAG3′tsRNA was highly expressed from mouse liver tumors compared to normal liver (Extended Data Fig. 2g), we studied the potential anti-tumor effect of an anti-Leu3′tsLNA in an orthotopic patient-derived HCC xenograft (PDX) model. Anti-Leu3′tsLNA administered during a 4-week period showed significantly reduced tumor growth (Extended Data Fig. 2h) and final xenograft volumes (Fig. 2c and Extended Data Fig. 2i) compared to saline and control LNA groups. LeuCAG3′tsRNA, but not mature tRNA, was nearly completely inhibited by anti-Leu3′tsLNA treatment (Extended Data Fig. 2j). No overall toxicity was observed based on stable body weights of treated mice (Extended Data Fig. 2k). A TUNEL assay demonstrated substantial apoptosis in treated xenograft tissues (Fig. 2d), consistent with our observations in cultured cells. These results show that inhibition of LeuCAG3′tsRNA induces apoptosis in tumor but not normal liver cells *in vivo*.

LeuCAG3′tsRNA inhibition impairs ribosome biogenesis

Although a recent study suggested 3′tsRNAs function like miRNAs[13], our experiments detected no such function for the Leu3'tsRNA (Extended Data Fig. 3a–c). In addition, RNA-seq profiles showed no global changes in mRNA transcription from LeuCAG3′tsRNA-inhibited cells (Extended Data Fig. 3d).

To investigate a possible relationship of the LeuCAG3′tsRNA and translation, we quantified the number of polysomal and ribosomal subunits in different conditions by sucrose gradient fractionation. While polysome fractions remained similar, the abundance of 40S and 80S ribosomal complexes was substantially decreased, and the relative abundance of 60S subunits increased, in LeuCAG3′tsRNA-inhibited cells compared to the control (Fig. 3a). Puromycin dissociation of 80S and polysomal ribosomes into free 40S and 60S subunits[21] revealed that the LeuCAG3′tsRNA-inhibited cells had 58.1±1.1% and 90.7±5.7% of the 40S and 60S subunits compared to the control, respectively (Fig. 3b). In agreement with the decrease in 40S ribosomal subunits, 18S mature rRNA abundance decreased to 66±6.2% in LeuCAG3′tsRNA-inhibited cells compared to control (Fig. 3c). Inhibition of other 5′ and 3′ tsRNAs did not affect the ribosome profiles (Extended Data Fig. 4a).

To distinguish if rRNA transcription and/or processing were affected upon LeuCAG3′tsRNA inhibition, we examined the abundance of different pre- and mature rRNAs by northern quantification in three cell lines (Fig. 3d and Extended Data Fig. 4b,c). Following inhibition of LeuCAG3′tsRNA, the 30S pre-rRNA accumulated to 205±16.7% of control while the 21S and 18S-E pre-rRNA signals decreased to 39.8% and 59.4%, respectively (Fig. 3d and Supplementary Table 3). However, the 32S pre-rRNA and the 45S primary transcript signals were only slightly increased. Together these results suggest that the LeuCAG3′tsRNA did not significantly affect either 28S mature rRNA processing or the abundance of the 45S primary transcript. Instead, a processing step resulting in the removal of the 5′ETS from the 30S intermediate was impaired, with a sequential reduction in the 18S rRNA.

As the LeuCAG3′tsRNA and anti-Leu3′tsLNA do not bind the rRNA precursors, this could not explain the rRNA processing changes (Extended Data Fig. 5a,b). Interestingly, the accumulation of 30S and the reduction of 21S and 18S-E pre-rRNAs, and 18S mature rRNA levels is a known consequence of reduced expression of specific small ribosomal proteins (RPS) such as RPS6, 7, 13, 16, 24, or 28[22]. We therefore reduced the concentration of these proteins or RPL7, XRN2 or c-MYC using siRNAs (Fig. 3d); the later two are important for rRNA biogenesis[23]. Depletion of RPS6, RPS13, or RPS28 but not the other proteins phenocopied the 5′ETS processing defect induced by the anti-Leu3′tsLNA, suggesting a possible functional relationship (Fig. 3d). Using western blotting, we measured the abundance of several ribosomal proteins known to affect the 5′ETS1-mediated rRNA processing (Fig. 4a) after LeuCAG3′tsRNA reduction. All the RPL proteins were excluded because they are required for 28S not 18S rRNA maturation[22]. Of the RPs evaluated, only RPS28 was substantially down-regulated relative to the control in LeuCAG3′tsRNA-inhibited cells (Fig. 4a), and the nuclear-cytoplasmic ratio of RPS6 and RPS28 was not altered (Extended Data Fig. 6a). RPS28 protein levels were also reduced in anti-Leu3′tsLNA-treated PDX liver tumors (Extended Data Fig 6b,c). The reduction in the expression of some RPS proteins (e.g. RPS13, RPS19, and RPL11) or other defects in rRNA biogenesis induce apoptosis[24,25]. Reducing RPS28 also resulted in apoptosis (Fig. 4b and Extended Data Fig. 6d). We were able to substantially rescue the tsRNA knockdown phenotype by co-transfection of the anti-Leu3′tsLNA and an RPS28 expression plasmid (Fig. 4c and Extended Data Fig. 6e–h) that increased protein levels by ~3× (compared to a EGFP control plasmid). Specifically, the increase in RPS28 expression in anti-Leu3′tsLNA-treated cells increased cell viability from 45% to 76% (Fig. 4c and Extended Data Fig. 6e) and reduced the accumulation of 30S rRNA precursor from 164.2±16.1% to 127.0±16.2%, resulting in the recovery of the 18S mature rRNA from 67% to 93% (Extended Data Fig. 6f–h). Collectively, our results suggest that the phenotypic effect of LeuCAG3′tsRNA knockdown is the result of lower RPS28 expression, which in turn impairs 18S rRNA maturation and ultimately induces apoptosis.

Because the inhibition of LeuCAG3′tsRNA reduced RPS28 protein abundance (Fig. 4a and Extended Data Fig. 6a–c) and not the *RPS28* mRNA levels in HeLa cells and the PDX HCC model (Fig. 4d and Extended Data Fig. 6i), we elected to study the polysomal sedimentation of various ribosomal protein and control mRNAs (Fig. 4e and Extended Data Fig. 7). Inhibition of the LeuCAG3′tsRNA selectively shifted the *RPS28* mRNA peak association

from 3–4 ribosomes (fraction #10) to 2 ribosomes (fraction #8); *GAPDH* and other control mRNAs were not significantly shifted (Fig. 4e and Extended Data Fig. 7). These results suggest that the tsRNA has a role in the translation of *RPS28* mRNA.

LeuCAG3′tsRNA enhances translation by binding mRNA

We established a direct physical interaction of the LeuCAG3′tsRNA and RPS28 mRNA using a modified cross-linking chromatin isolation by RNA purification assay[26,27] (Extended Data Fig. 8a). We identified two potential LeuCAG3′tsRNA binding sites in the *RPS28* mRNA using RNAhybrid[28] (Extended Data Fig. 8b). mRNA secondary structure prediction programs (RNAfold, mfold, and RNAstructure)[29–31] and minimal free energy calculations implied target1 (in the 3′ UTR) forms a duplex with a ~22-nt region that overlaps the translation initiation site (anti-target1), while target2 (in the coding sequence) is a hairpin structure (Fig. 5a). We hypothesized that the tsRNA binds *RPS28* mRNA to enhance translation, perhaps by unfolding the mRNA secondary structure through competition with folding of target sites (Extended Data Fig. 8c). We constructed expression plasmids containing either a wild-type (wt) or variant *RPS28* mRNA sequences that maintained the same protein coding sequence but disrupted the tsRNA-*RPS28* mRNA interaction in order to negate the effect of LeuCAG3′tsRNA on mRNA translation (Fig. 5a). We co-transfected each plasmid with either the anti-Leu3′tsLNA or control LNA in HeLa cells. RPS28 mRNAs harboring mutants in the anti-target1 (A) or target2 (C) regions lost their ability to respond to altered cellular levels of the tsRNA. In contrast, RPS28 mRNAs containing similar nucleotide changes outside the target sites (B and D) responded in the same manner as the wild-type mRNA to the varied concentration of the tsRNA (Fig. 5b and Extended Data Fig. 8e). Similar results were obtained using C-terminal flag-tagged versions of the same RPS28 wt and mutant expression plasmids that allowed us to distinguish the newly synthesized RPS28 protein from total RPS28 protein in the whole cellular pool (Fig. 5b and Extended Data Fig. 8e,f).

To corroborate the genetic complementation data, we synthesized the variant *RPS28* mRNAs and tested them for translation in a cell-free rabbit reticulocyte system with or without the addition of the synthetic tsRNA. Synthetic LeuCAG3′tsRNA enhanced translation of the wt *RPS28* mRNA but not the firefly luciferase and Xenopus elongation factor1 (Xef1) mRNAs (Extended Data Fig. 8g–i). Importantly, mRNA translation from mutants A and C were not enhanced relative to the wt or mutant B mRNA in the presence of the LeuCAG3′tsRNA (Fig. 5c and Extended Data Fig. 8j). To ensure that LeuCAG3′tsRNA enhances *RPS28* mRNA translation by base-pairing with the target2 site, we used the modified target2 sequence (mutant C) RPS28 mRNA for *in vitro* translation but added a sequence-modified tsRNA mimic designed to be nearly complementary to the modified target2 site (mutant C). This compensatory tsRNA enhanced the translation of mutant C but not wt *RPS28* mRNA (Fig. 5d and Extended Data Fig. 8k). These experiments strongly support that binding of LeuCAG3′tsRNA affects RPS28 translation through base-pairing interactions at target sites within the mRNA.

LeuCAG3′tsRNA target prediction

To determine whether LeuCAG3′tsRNA can modulate the translation of other mRNAs, we first selected mRNAs where the CDS and flanking 30 bp were nearly complementary to LeuCAG3′tsRNA based on the minimal free energy[28] (Extended Data Fig. 9a). Target sites contained in a UTR might affect translation by forming secondary structures with distal coding sequences. However, because current algorithms cannot accurately predict the secondary structure of longer mRNAs[32] we excluded potential target sites in UTR regions fully outside of the CDS by >30 nt. Interestingly, we found ribosomal proteins RPS9, 14, and 15 mRNAs contained prospective target sites in their CDS (Extended Data Fig. 9b,c). To estimate if the target sites were in a duplexed RNA structure, we analyzed the secondary structure of the target site using *in vivo* click selective 2′-hydroxyl acylation and profiling (icSHAPE) data in living cells[33]. This showed target1, anti-target1, and target2 sites in the *RPS28* mRNA primarily exist in a double-stranded state (Extended Data Fig. 9d) as foreseen by RNAhybrid (Fig. 5a) and other prediction programs. The icSHAPE result also showed that the predicted RPS15 mRNA target is double-stranded (Extended Data Fig. 9d). RPS15 is involved in a later step of 18S ribosomal RNA processing, and its depletion does not affect mature 18S rRNA abundance[22]. The target sites in *RPS9* and *14* mRNAs were primarily located in a single-stranded region (Extended Data Fig. 9d). We hypothesized that translation of the RPS15 but not RPS9 and 14 mRNAs would be influenced by the concentration of the LeuCAG3′tsRNA.

The presence of LeuCAG3′tsRNA enhanced *RPS15* mRNA translation in HeLa cells and the PDX HCC tumor model (Extended Data Fig. 10a–e). In contrast, RPS9 and 14 protein levels were not significantly different after ASO/LNA-mediated reduction of the tsRNA (Extended Data Fig. 10f,g). Plasmids expressing either wild-type or target variant *RPS9, 14,* and *15* mRNA sequences (similar to what was done for target variant *RPS28* mRNA) were co-transfected with either anti-Leu3′tsLNA or control LNA in HeLa cells (Extended Data Fig. 10f–i). The RPS15 target-site mutant mRNA lost its responsiveness to tsRNA inhibition (Extended Data Fig. 10h,i). However, translation of wild-type and target-site RPS9 and 14 mRNAs remained unchanged regardless of the tsRNA concentration (Extended Data Fig. 10f,g). *In vitro* translation assays with RPS15 mRNA corroborated these genetic complementation data by showing that LeuCAG3′tsRNA enhanced translation from the wild-type and non-target mutant RPS15 mRNAs, whereas no change was observed with the RPS15 target-site mutant mRNA (Extended Data Fig. 10j,k). We propose that the LeuCAG3′tsRNA is involved in unfolding the mRNA target sites that have duplexed secondary structures allowing for enhanced translation.

The specific tsRNA studied here fine tunes the production of at least two ribosomal proteins and ultimately the number of ribosomes in proliferating cells. Decreasing the production of individual ribosomal proteins did not have a major effect on global protein synthesis (Extended Data Fig. 1g), a finding consistent with previous studies[34,35]. Our studies establish how a non-coding RNA positively regulates mRNA translation. Further investigation is required to establish how the 3′tsRNA is generated and regulated in normal and disease states, the mechanism of target site recognition, and the process of translational regulation. The presence of hundreds of different tsRNAs suggests they have a biological

role in cells, perhaps in similar or different post-transcriptional gene regulatory pathways that might involve altering RNA secondary structures. The relatively high concentration of LeuCAG3′tsRNA in tumors and immortalized cells, and the induction of apoptosis in such cells when the tsRNA is reduced, warrants additional evaluation as a potential therapeutic target in treating cancer.

Methods

Cell Culture and Transfection

HeLa, HCT-116, and HEK293T cells were purchased from ATCC and were grown in Dulbecco's modified Eagle's medium (DMEM; GIBCO-BRL) with 2 mM of L-glutamine, and 10% heat-inactivated fetal bovine serum with antibiotics. All cells were negative for mycoplasma. 30–60 nM of locked nucleic acid (LNA) mixmers, 10–30 nM of LNA gapmers, 100 nM of synthetic tsRNAs, and/or plasmids were transfected using Lipofectamine 2000 (Life Technologies) according to the manufacturer's instructions. LNA oligos (Supplementary Table 4) were synthesized by Exiqon. DNA (Supplementary Tables 4 – 7 and 9) and synthetic tsRNA (Supplementary Table 4) oligos were synthesized by IDT. The siRNAs were purchased from Dharmacon or Life Technologies.

Establishment of orthotopic HCC patient-derived xenografts and treatment with LNAs

Patient samples were obtained, with signed informed consent, from a study approved by the Institutional Review Board (IRB) at Stanford University. The HCC patients underwent liver resection as part of their routine treatment. Some of the resected tumors were used to establish patient-derived HCC xenografts under the protocols approved by the IRB and the Stanford University Administrative Panels on Laboratory Animal Care. Animal studies were carried out in compliance with federal and local institutional rules for the conduct of animal experiments. Patient-derived HCC xenografts were established as previously described[36]. Briefly, single tumor cells labeled with a luciferase expression vector were suspended in BEME medium containing 50% Matrix Matrigel, and then subcutaneously injected into 4- to 8-week old NOD.Cg-Prkdc^{scid}Il2rg^{tm1Wjl}/SzJ (Nod-SCID-Gamma; NSG) mice (Jackson Laboratory; Bar Harbor, MA) (20–25 g body weight). Tumor development was monitored daily. Once the subcutaneous xenograft reached 1 cm in diameter, it was removed and cut into 2 mm^3 pieces and surgically implanted into the left lobe of the liver of 6-week old NSG mice. Tumor growth was monitored by bioluminescence imaging using the Xenogen IVIS *in vivo* imaging system (Caliper Life Sciences, Hopkinton, CA), until the tumors were established (usually one week after tumor implantation). Mice with similar tumor bioluminescence signals were selected and randomized into groups (n = 10 for each group) for intraperitoneal injection with saline (control), con LNA (0.6 mg/kg), or anti-Leu3′ts LNA (0.6 mg/kg) every 2 to 3 days. The LNAs used for injection were phosphorothioate modified. Tumor growth was monitored weekly by bioluminescence imaging, and growth curves were plotted using average bioluminescence within each group. Body weight was also measured every 2 to 3 days. After 4 weeks of treatment, the mice were sacrificed and the tumors and normal livers harvested. Tumor size was measured with digital calipers and tumor volume was calculated using the formula $\pi/6 \times$ larger diameter $\times$ [smaller diameter]^2. Liver and tumor tissues were fixed in formalin and embedded with paraffin.

Alanine transaminase (ALT) measurements

BALB/cJ mice (6- to 8-weeks old) were randomized into groups (n = 2–3 each). The LNAs used for injection were phosphorothioate modified. After hydrodynamic injection of saline, 125 ug of con LNA or anti-Leu3′tsLNA[37,38], mouse serum was collected by centrifugation of whole clotted blood that was obtained by retro-orbital bleeding at indicated day (Extended Data Fig. 2e). Alanine aminotransferase (ALT) levels were measured using an ALT kinetic measurement kit (Teco Diagnostics).

Plasmid constructs

Complementary sense and anti-sense primers used for cloning were synthesized by IDT (Integrated DNA Technologies) (Supplementary Table 5). The dimers were cloned into the 3′ UTR or 5′ UTR of the pGL3 control luciferase plasmid using XbaI and EcoRI or HindIII and NcoI enzymes, respectively. The *Renilla* gene from the psiCHECK-2 plasmid (Promega), for which all the CUG codons were replaced by CUU or CUC codons, was synthesized by Life Technologies. The full-length RPS9 gene was amplified with primers (5′-ctctttctcagtgaccggg-3′ and 5′-agcgctgatcctgtttatttg-3′). The full-length RPS14 gene was amplified with primers (5′-ctccgccccctcccactctc-3′ and 5′-tttttgaaacagtttacatgaaggc-3′). The full-length RPS15 gene was amplified with primers (5′-ggcagtctcgcgataactgc-3′ and 5′-agtcatgtgcgcctttattag-3′). The full-length RPS28 gene was amplified with primers (5′-ctctccgccagaccgccgc-3′ and 5′-ttttttttttttttttttttttaacttgaaacacaaacgctt-3′). The full-length RPS9, 14, 15, 28 protein sequences were cloned into the pcDNA3.3 plasmid. C-terminal flag tagged containing RPS28 sequences were generated using site-directed mutagenesis. The CMV promoter was replaced by the human PGK promoter. Site-directed mutagenesis was performed with the QuikChange II XL Site-Directed Mutagenesis Kit (Stratagene) to generate point mutations or deletions in the recombinant RPS9, 14, 15, and 28 genes (primers in Supplementary Table 9). All plasmid clones were confirmed by DNA sequencing.

Dual-Luciferase Reporter Assay

Both pGL3 and pRL plasmid DNA, or psiCHECK-2 plasmid DNA were co-transfected with 60–100 nM of LNA into Hela or HCT-116 cells in 24 well plates. FF-luciferase and RL-luciferase activities were measured 24 h after transfection by using Promega's dual-luciferase kit protocol and luminescence was detected using a Modulus Microplate Luminometer (Turner BioSystems). Firefly or *Renilla* luciferase activity from pGL3 plasmid or psiCHECK-2 plasmid were normalized with the co-transfected *Renilla* activity from pRL or firefly activity from psiCHECK-2, respectively. The values obtained in the anti-Leu3′tsLNA co-transfected cells were normalized to the con co-transfected cells. All experiment were performed in triplicate.

RNA isolation and northern blotting

Total RNA was isolated with TRIZOL reagent (Life Technologies) according to the manufacturer's instructions. Total RNA was resolved by electrophoresis on a 15% (w/v) polyacrylamide gel with 7 M urea for detection of small RNAs <200 bp or on a 0.9% agarose denaturating gel for detection of large RNAs (>200 bp). The RNA was transferred

onto a Hybond-N+ nylon membrane (Amersham). P^{32}-labeled oligonucleotides or amplified cDNA probes were hybridized to the membrane in PerfectHyb Plus hybridization buffer (Sigma). All antisense oligonucleotides for northern probes are listed on Supplementary Table 4. All oligonucleotides for the generation of cDNAs as northern probes are listed in Supplementary Table 6.

Measurement of cell proliferation

Cell proliferation was measured with a CellTiter 96 nonradioactive cell proliferation assay kit (MTS assay; Promega) according to the manufacturer's instructions. All experiments were performed in triplicate.

Apoptosis assay

The cell apoptosis assay was performed by measuring translocation of membrane phospholipid phosphatidylserine using an Annexin V-FITC apoptosis detection kit (BD Pharmingen) according to the manufacturer's instructions. Cells were analyzed using a FACScalibur instrument using FlowJo software (Tree Star). For the TUNEL assay, the apoptotic responses were identified 24 h post-transfection using Invitrogen's Click-iT TUNEL Alexa Fluor 594 Imaging Assay kit according to the manufacturer's instructions. For the TUNEL staining of paraffin embedded 6 m tissue sections, ApopTag Peroxidase In Situ Apoptosis Detection Kit (EMD Millipore) was used according to the manufacturer's instructions.

Western blotting

24 h post-transfection, cell lysates were prepared using 1× cell lysis buffer (Cell Signaling) with 1 mM PMSF (Cell Signaling). 6–10 ug of protein lysate was run on a 4–20% SDS PAGE and transferred to Hybond-P or nitrocellulose membrane (GE Healthcare). The membrane was incubated for 20 min at room temperature (RT) in a 4% BSA (Omnipur) solution, washed, and incubated overnight (O/N) at 4 °C with one of the antibodies listed below. After washing and incubation for 1 h at RT with secondary antibody, the protein signal was detected using a Pierce ECL2 substrate (Thermoscientific) or Odyssey CLx imaging system (LI-COR Biosciences) according to the manufacturer's instructions. Antibodies for immunoblotting were as follows: anti-PARP rabbit monoclonal Ab (clone 46D11; Cell Signaling), anti-cleaved PARP (Asp214) rabbit monoclonal Ab (clone D64E10; Cell Signaling), anti-GAPDH-peroxidase mouse Ab (Sigma), anti-RPS13 rabbit polyclonal Ab (Abnova), anti-RPS7, 10, 16, 19, 24, and 28, XRN2 Ab (Abcam), anti-RPS9, 14, and 15 Ab (Aviva), RPL7, 13a, 26, and XRN2 Ab (Abcam), anti-RPS6 mouse monoclonal Ab, anti-flag Ab (Cell signal).

High throughput large RNA sequencing

24 h post-transfection, total RNA was isolated using the TRIZOL reagent. Residual DNA contamination and ribosomal sequences were removed from total RNA using TURBO DNA-free Kit (Life Technologies) and Ribo-Zero Gold kit (Epicentre) respectively according to the manufacturer's instructions. A total of 150–200 ng of purified RNA was subjected to strand-specific RNA-seq using the ScriptSeq v2 mRNA-SEQ library preparation kit

(Epicentre), which uses a random-hexamer method of cDNA synthesis according to the manufacturer's instructions. 50-bp paired-end reads were generated on an Illumina HiSeq 2000 machine yielding a total of 18 to 40 million paired-end reads. Sequences were mapped to the human hg19 genome using TopHat version 1.4.1 with the following parameters: -r 180, --mate-std-dev 130 –library-type fr-secondstrand[39]. FPKM values were calculated using the CuffDiff program version 1.3.0[40,41] using refGene transcripts as an input file for comparison of gene expression levels. Sequences have been deposited in the NCBI Gene Expression Omnibus (accession number GSE54878).

Real time PCR

500 ng of total RNA was reverse transcribed with the superscript II RT kit (Life Technologies) and subjected to gene expression analyses with gene-specific TaqMan probes (4326317E for GAPDH, Hs04195024_g1 for RPS6, Hs01652370_gH for RPS10, HS01358643_g1 for RPS15, either HS02597256_g1 or HS02597258_g1 for RPS28). Real time PCR was performed on a CFX384 Real-Time system (Bio-Rad). All experiments were performed in triplicate. All mRNA levels were normalized to *GAPDH* mRNA.

Polysome gradient and RNA preparation

Polysome gradient and RNA preparation were performed as described previously[42] with modifications. 24 h post-transfection, cells were treated with 100 μg/ml of cycloheximide (Sigma-Aldrich) for 3 min, and cells were lysed in buffer containing 15 mM Tris–HCl (pH 7.5), 150 mM KCl, 5 mM $MgCl_2$, 500 U/ml RNasin (Promega), and 1% Triton X-100. The cleared lysates were loaded onto 10–50% sucrose gradients (15 mM Tris–HCl (pH 7.5), 150 mM KCl, 5 mM $MgCl_2$, 20 U/ml SUPERaseIn (Life Technologies), and 100 μg/ml cycloheximide with a 60% sucrose cushion. Gradients were centrifuged at 35,000 rpm at 4 °C for 2 h 45 m and fractionated with a Teledyne Isco Foxy R1 Retriever/UA-6 detector system. The gradient fractions were sequentially treated for 30 min at 37 °C with 0.5 mg/ml proteinase K (New England Biolabs) in the presence of 5 mM EDTA. RNAs were extracted with an equal volume of phenol–chloroform–isoamylalcohol (25:24:1; Life Technologies), re-extracted with chloroform, and ethanol precipitation was performed.

Puromycin gradients

Puromycin gradients were performed as described previously[42] with modifications. 24 h post-transfection, cells were lysed in buffer containing 15 mM Tris–HCl (pH 7.5), 500 mM KCl, 2 mM $MgCl_2$, 2 mM puromycin, 500 U/ml RNasin (Promega), 20 U/ml SUPERaseIn (Life Technologies), and 1% Triton X-100. Following incubation on ice for 15 min, 80S ribosome subunits were separated at 37 °C for 10 min. Following centrifugation, cleared lysates were loaded onto 10–50% sucrose [500 mM KCl, 15 mM Tris–HCl (pH 7.5), 2 mM $MgCl_2$, and 20 U/ml SUPERaseIn (Life Technologies)] with a 60% sucrose cushion. Gradients were centrifuged at 35,000 rpm at 4 °C for 2 h 45 min.

Metabolic labeling of cell proteins with [^{35}S]-Methionine

24 h post-transfection, cells were washed twice with PBS and grown in DMEM media without Cystine and Methionine (DMEM -Cys-Met) (Life Technologies) for 30 min at

37 °C. The media was removed and DMEM -Cys-Met media plus 100 μCi protein labeling mix (Perkin Elmer) was added for 10 min at 37 °C. Cells were washed twice with cold PBS, harvested, and lysed with RIPA buffer. Equal amounts of protein were resolved on 4–12% SDS-PAGE, stained with Coomassie brilliant blue, the gel was dried, and the incorporated radioactivity was scanned using a PMI (Personal Molecular Imager).

Immunoprecipitation

Antibodies were incubated with protein A/G UltraLink Resin (Thermo Scientific) overnight at 4 °C. Cells were lysed with IP buffer (25 mM Tris pH7.5, 150 mM KCl, 0.5% NP40, 0.02 mM EDTA) containing RNasin plus (Promega) and cOmplete Protease Inhibitor Cocktail Tablets (Roche) and incubated with prepared protein A/G conjugated Antibodies for 2 h at 4 °C. All samples were washed with IP buffer 3 times. Immunoprecipitated RNAs were extracted using TRIZOL (Life Technologies) according to the manufacturer's instructions. Immunoprecipitated proteins were separated from protein A/G UltraLink resin by adding RIPA buffer and boiling for 5 min. Antibodies for immunoprecipitation were as follows: anti-Ago1 monoclonal Ab (clone 1F2; Wako), anti-Ago2 monoclonal Ab (clone 2D4; Wako), and anti-Ago3 monoclonal Ab (clone 1C12; Wako).

Modified cross-linking chromatin isolation by RNA purification assay (ChIRP) assay

The modified ChIRP assay was performed as described earlier[26,27] with slight modifications. After transfection of the synthetic LeuCAG3′tsRNA into cells, RNA cross-linking was performed and the *RPS28* or *GAPDH* mRNAs were pulled down with 4 and 14 biotinylated tiling oligonucleotides (Supplementary Table 7), respectively. Specifically, after transfection of 6 nM of synthetic LeuCAG3′tsRNA, 293T cells were cross-linked with 3.7% formaldehyde and sonicated with a Qsonica sonicator with the following settings: 15 s pulse with 15 s between each pulse; 75% ampl for 1 min at 4 °C. The cleared lysate was then hybridized with 14 and 4 biotinylated tiling oligos against GAPDH and RPS28 mRNAs, respectively (sequences in Supplementary Table 7). After a 4 h hybridization, the streptavidin beads were hybridized together for 1 h, washed 6 times, and subjected to phenol-chloroform extraction. Extracted RNA was used for RT-PCR to detect GAPDH and RPS28, and resolved on a 15% denaturing gel to detect the LeuCAG3′tsRNA.

In vitro translation

Each mRNA was synthesized using T7 MEGAscript (Life Technologies). *In vitro* translation using the Flexi Rabbit Reticulocyte Lysate System (Promega) was performed according to manufacturer's instructions with minor modifications. Briefly, 100 ng of luciferase mRNA, or 60 ng of both RPS28 mRNA and Xef1 mRNA were mixed in 15 μl of translation reaction containing 70% of reticulocyte lysate. The indicated amounts or 14 pmol of synthetic LeuCAG3′ts RNA or control RNAs were added to the reaction and incubated for 30–45 min at 30 °C. Firefly luciferase activity was measured with a Luciferase Assay System (Promega). RPS28 and Xef1 products were resolved on 4–12% SDS PAGE, exposed with a phosphor image screen, and quantified.

mRNA structures and structure probing of tsRNA targets

The m.f.e. is minimal free energy between the LeuCAG3′tsRNA and binding site in each mRNA, was predicted using a RNA-hybrid program (https://bibiserv2.cebitec.uni-bielefeld.de/rnahybrid). The *RPS28* mRNA secondary structure was predicted by RNAfold (http://rna.tbi.univie.ac.at) and we retrieved icSHAPE data from a previous study allowing us to experimentally predict the each mRNA structure[33]. This approach allowed us to probe the nucleotide reactivity (i.e., single-strandness) in HEK293T cells. While this study was performed in whole treated cells, we also obtained cytoplasmic RNA structure data from an unpublished study that separated and measured RNA structures in different cellular fractions with icSHAPE.

Statistical information

All data are presented as mean ± S.D. Data were analyzed with two-tailed Student's *t*-test in PRISM 6.0. A *P*-value of 0.05 or lower was considered significant.

Data availability

All data generated or analysed during this study are available from the authors and/or are included in this published article and online supplementary information). Data from RNA-seq have been deposited in the NCBI Gene Expression Omnibus (accession number GSE54878).

Extended Data

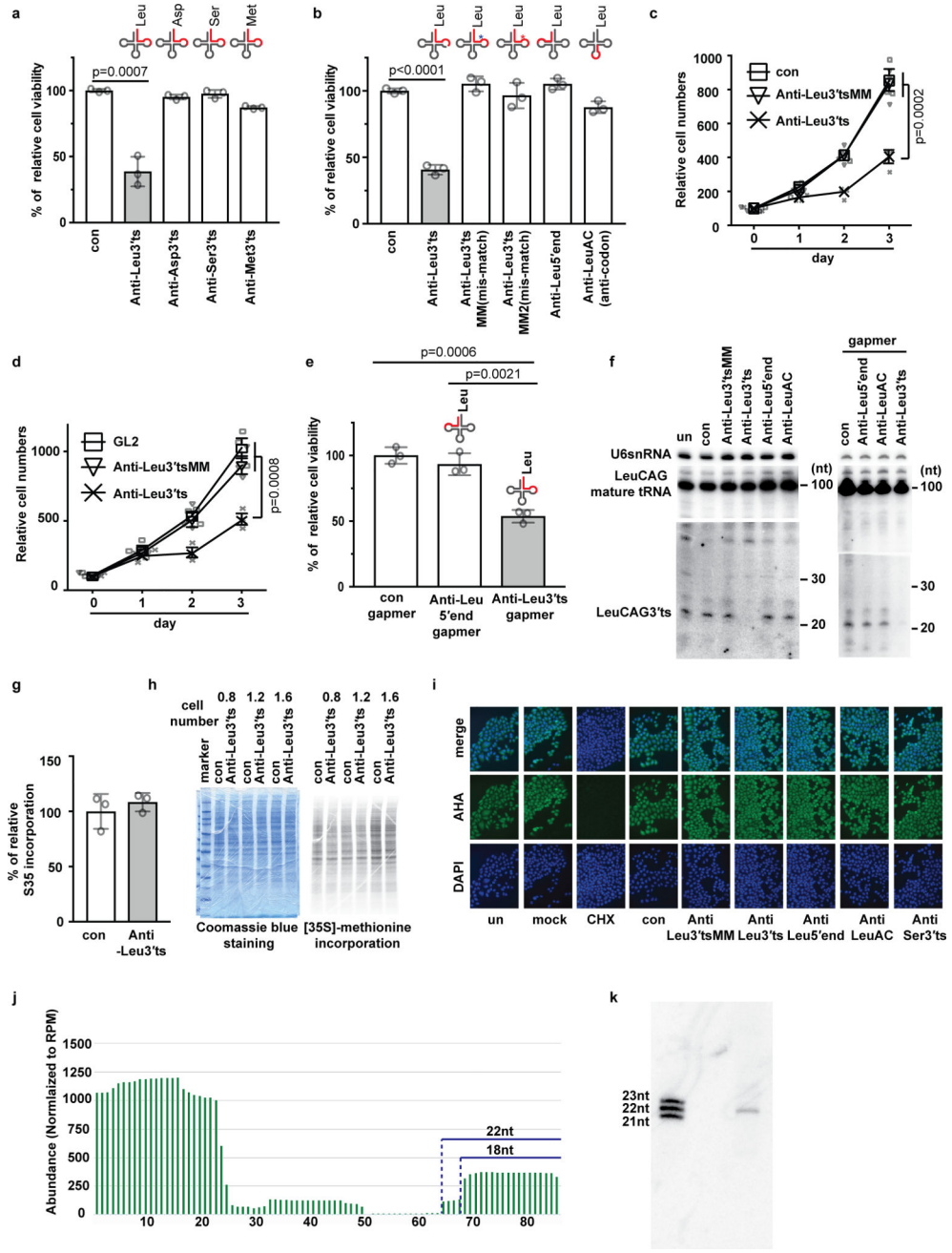

Extended Data Figure 1. 22-nt LeuCAG3′tsRNA is involved in cell viability

a, b, Inhibition of LeuCAG3′tsRNA impairs HCT-116 cell viability. 3 days post-transfection, a MTS assay was performed (n=3 independent experiments). Each LNA is perfectly complementary to colored region on the tRNA diagram above each bar. Blue and red asterisk mark, different 2-nt mismatches. **c, d,** Inhibition of the LeuCAG3′tsRNA decreased the number of viable HeLa (c) and HCT-116 cells (d) (n=3 independent experiments). The cell number at each day was normalized to the day zero value. **e**, Cleavage of LeuCAG3′tsRNA impairs HeLa cell viability. 3 days post-transfection, a MTS

assay was performed as in (a) (n=3 independent experiments). **f**, Northern analysis of the LeuCAG3′tsRNA and mature Leu-tRNA post-transfection. To quantify the tsRNA and mature tRNA level correctly, transferred blots were cut at the 40–50 nt position and hybridized with the same probe to detect tRNA (top) and tsRNA (bottom) separately (n=2 independent experiments). U6 snRNA, the loading control. **g**, 24 h post-transfection, global protein synthesis assay using [^{35}S]-methionine metabolic labeling in HeLa cells (n=3 independent experiments). **h,** 24 h post-transfection, global protein synthesis detection on gels using [^{35}S]-methionine metabolic labeling in HeLa cells. Coomassie brilliant blue (left) as a loading control; gels were scanned to measure incorporated radioactivity (right) (n=2 independent experiments). Each number multiplied by 10^5, the number of cells on 6-well culture dishes 24 h prior to transfection. **i,** Global protein synthesis assay using a Click-iT AHA (L-Azidohomoalanine) Alexa Fluor 488 assay in HeLa cells was performed 24 h post-transfection. The nucleus was stained with DAPI, blue color. Protein synthesis was measured with AHA, green color. Merge represents the DAPI and AHA merged images (n=2 independent experiments). Un, untreated cells; mock, transfection without LNA; CHX, cycloheximide-treated positive control. **j**, The abundance of sequencing reads aligned to LeuCAG-tRNA from HeLa cells. This analysis was generated from tRFdb (http://genome.bioch.virginia.edu/trfdb/search.php). X-axis, a position on LeuCAG mature tRNA. Blue line, the 18 and 22 nt of LeuCAG 3′tsRNAs. **k**, The LeuCAG3′tsRNA major isoform is 22 nt. A northern hybridization was performed. The 18-nt isoform was not detected (n=2 independent experiments). Mean is indicated. Error bar, s.d.; indicated p-value by two-tailed t-test (a–e).

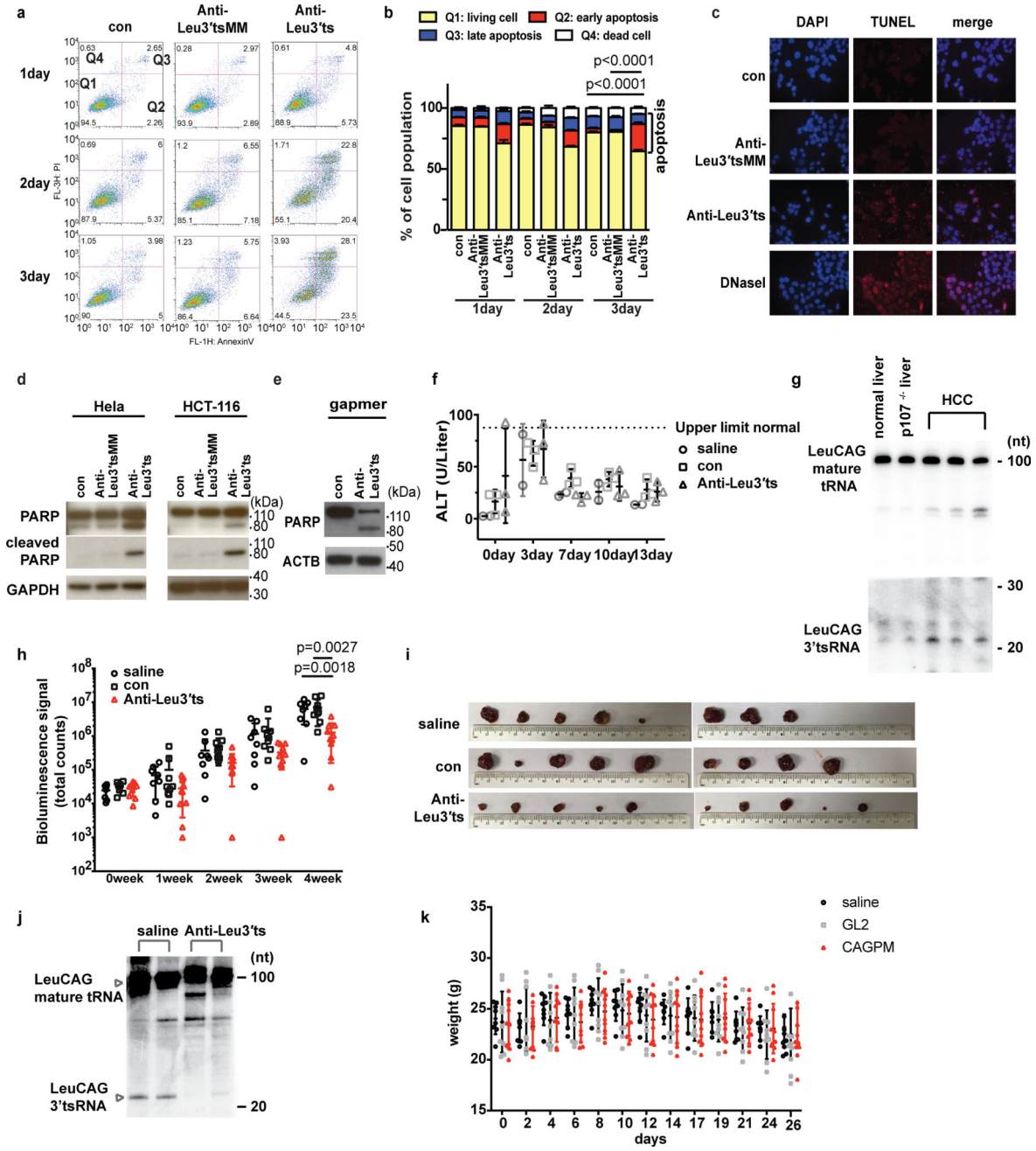

Extended Data Fig. 2. Inhibition of LeuCAG3′tsRNA induces apoptosis *in vitro* and inhibits the growth of hepatocellular carcinoma (HCC) patient-derived xenograft

a, A representative result of the apoptosis assay. Apoptosis in HeLa cells was measured using Annexin V-FITC and PI staining at 24, 48 and 72 h post-transfection. The percentage of cells was shown in each gate. Q1 (Healthy cells), stained with neither Annexin V nor PI; Q2 (early apoptotic cells), positive with Annexin V; Q3 (late apoptotic cells), positive with Annexin V and PI; Q4 (dead cells), positive with PI. The average cell population of the apoptosis assay is provided in Fig. 2a (n=3 independent experiments). **b,** Inhibition of the LeuCAG3′tsRNA results in increased apoptosis in HCT-116 cells. The apoptosis assay was

done as in **(a)** (control at 1 d, n=2; all other samples, n=3 independent experiments). **c,** Inhibition of LeuCAG3′tsRNA causes DNA fragmentation in HCT-116 cells. A TUNEL assay was performed 24 h post-transfection. DNase I is a positive control. TUNEL-positive cells are stained red. Merge is DAPI and TUNEL merged staining (n=2 independent experiments). **d, e**, Inhibition (mixmer LNA) (d) and cleavage (gapmer LNA) (e) of LeuCAG3′tsRNA causes PARP protein cleavage. Western blot analysis was performed 24 h post transfection. Anti-PARP Ab detects both full-length (116 kD) and cleaved (89 kD) PARP protein. ACTB is the loading control (n=2 independent experiments). **f,** For liver toxicity, 125 μg of each LNA (tsRNA sequence is the same in human and mouse) was injected into C57BL/6J mice by hydrodynamic tail vein injection (saline group, n=2; other group, n=3 independent mice). **g,** The LeuCAG3'tsRNA is highly expressed from mouse models of HCC generated from conditional TKO ($Rb^{lox/lox}$; $p130^{lox/lox}$; $p107^{-/-}$) adult mice[43]. Normal liver was harvested from C57/BL6 mice. Northern hybridization was performed as in Extended Data Fig. 1f (n=2 independent experiments). **h,** Over the 4-week study period, mice containing an orthotopic human xenotransplanted hepatocellular carcinoma were given intraperitoneal injections of: saline, con, and anti-Leu3′tsLNA. The luciferase signal as a marker of tumor growth was monitored weekly (saline group, n=8; con group, n=9; Anti-Leu3′ts group, n=10 independent mice). **i,** After the 4week injection period, all mice were sacrificed and tumors harvested. **j**, Anti-Leu3′tsLNA inhibits LeuCAG3′tsRNA *in vivo*. Northern hybridization was performed with total RNAs from saline or anti-Leu3′tsLNA injected mice (n=2 independent experiments). **k,** Body weight curve of individual mice bearing HCC xenografts during the 4-week experiment. (saline group, n=8; con group, n=9; Anti-Leu3′ts group, n=10 independent mice). Mean is indicated. Error bar, s.d.; indicated p-value by two-tailed t-test (b, h); p-value (b), early apoptosis population. For gel source data, see Supplementary Figure 1.

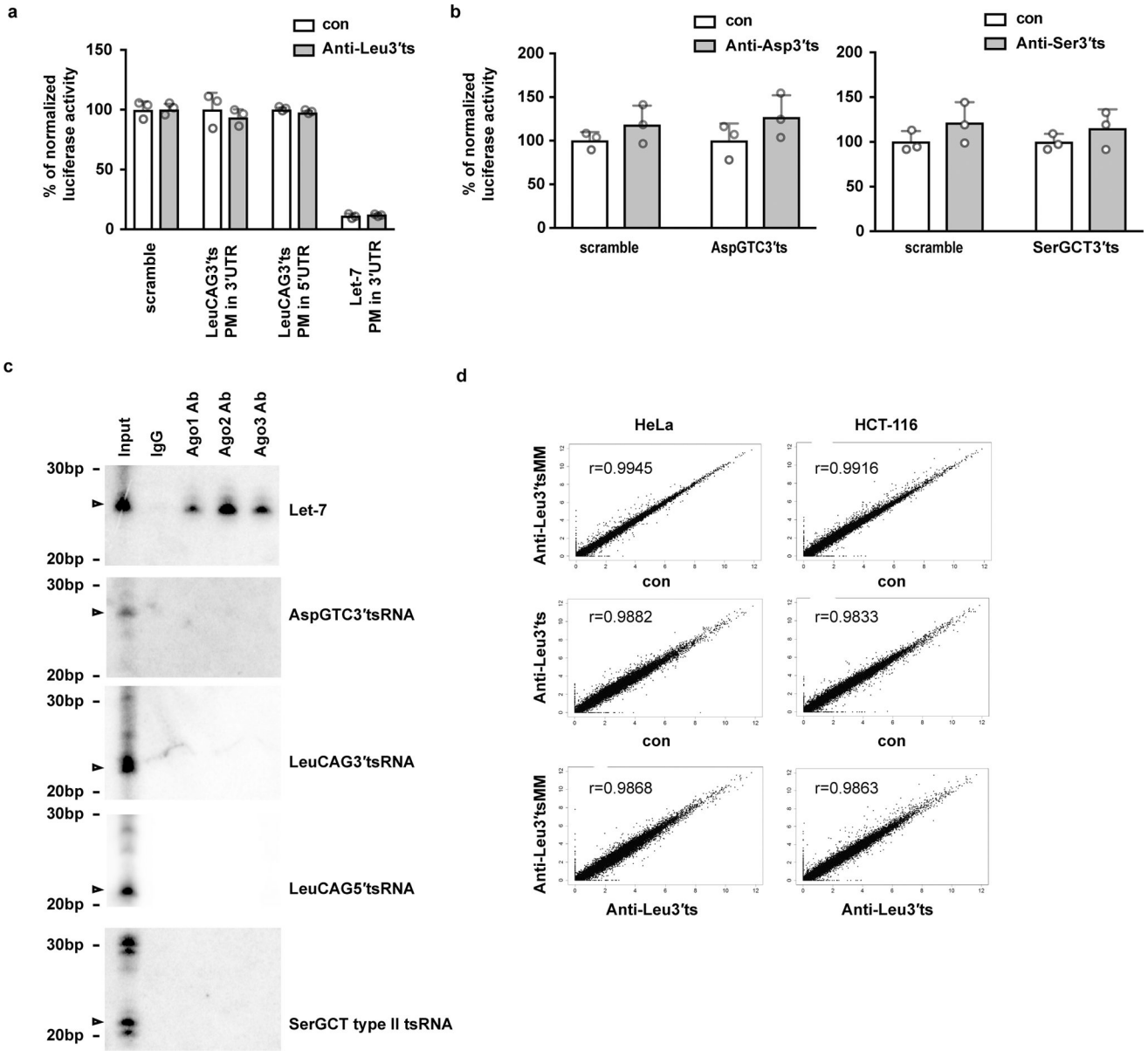

Extended Data Figure 3. LeuCAG3′tsRNA does not have transgene silencing activity

a, LeuCAG3′tsRNA does not repress luciferase gene expression containing perfect complementary target sites in its 3′ UTR or 5′ UTR. A luciferase plasmid (x-axis) was co-transfected with con or anti-Leu3′tsLNA (n=3 independent experiments). The normalization protocol is described in Methods. Scramble, scrambled sequences in 3′ UTR; LeuCAG3′tsPM in 3′ UTR, two copies of the perfect complementary sequence of the LeuCAG3′tsRNA in 3′ UTR; LeuCAG3'tsPM in 5′ UTR, two copies of the perfect complementary sequence of the LeuCAG3′tsRNA in 5′ UTR; Let-7 PM is a positive control, a single copy of perfect complementary sequences of the Let-7 miRNA in 3′ UTR. **b,** AspGTC3′tsRNA or SerGCT3′tsRNA does not repress luciferase gene expression in a construct that contains two copies of the corresponding perfect complementary target site in its 3′ UTR. A luciferase assay was performed as in (**a**) (n=3 independent experiments). X-

axis, target sites in the 3′ UTR. **c**, The tsRNAs are not associated with Ago proteins. Endogenous Ago1, 2, and 3 proteins were immunoprecipitated by the indicated Ab and the associated RNAs were subjected to northern blotting. The closed triangle in each northern blot indicates the detected tsRNA. IgG, control. Let-7 is a positive control (n=2 independent experiments). **d,** LeuCAG3′tsRNA does not affect global gene expression in HeLa and HCT-116 cells. Scatter plots comparing gene expression ($\log_2$ (FPKM+1)) of two RNA-Seq datasets from samples 24 h post-transfection (Supplementary Table 2). The Pearson correlation coefficient is indicated by the r value in each plot (n=1). Mean is indicated. Error bar, s.d. For gel source data, see Supplementary Figure 1.

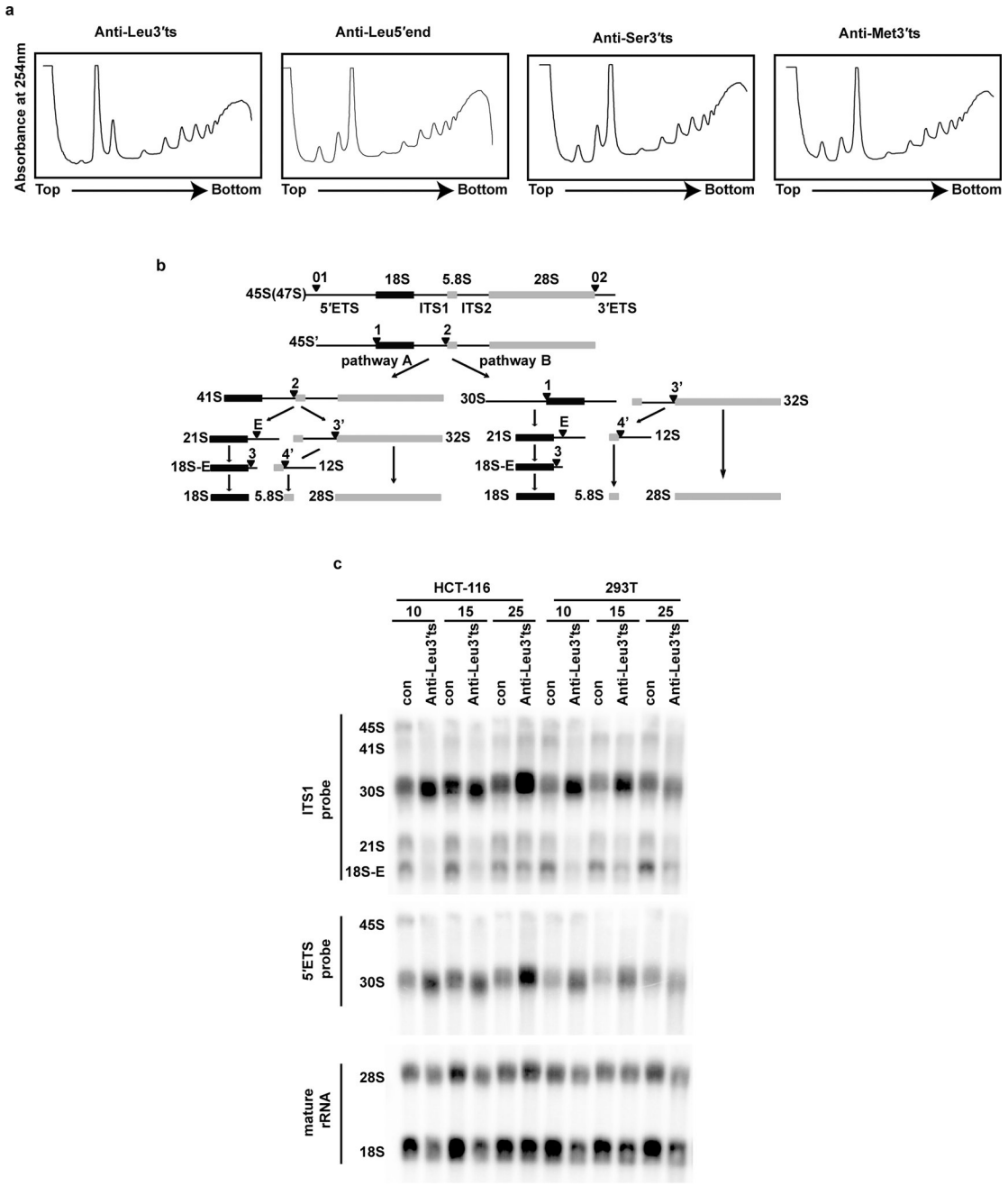

Extended Data Figure 4. LeuCAG3′tsRNA is a non-coding RNA required for ribosome biogenesis

a, LNAs directed against 5′ end of the LeuCAG-tRNA, Ser3′tsRNA (3′ end of the SerGCT-tRNA), and Met3′tsRNA (3′ end of the MetCAT-tRNA) does not change the ribosome/polysomal profiles. 24 h post-transfection cytoplasmic lysates from HeLa cells were treated with cycloheximide and separated on 10−50% sucrose gradients. The polysomal profile was analyzed as in Fig. 3a (n=2 independent experiments). **b,** Pre-rRNA processing pathways in human cells based on prior studies[45,46] is shown. The 45S primary transcript (pre-45S) is processed and categorized as: 5′external transcribed spacers (5′ETS), mature 18S rRNA, internal transcribed spacer 1 (ITS1), mature 5.8S rRNA, internal

transcribed spacer 2 (ITS2), mature 28S rRNA, and 3′external transcribed spacers (3′ETS). There are two alternative processing pathways. Inhibition of LeuCAG3′tsRNA inhibits processing from the 30S intermediate to 21S intermediate form depicted in pathway B. Arrowhead and number indicate cleavage sites. **c,** Inhibition of the LeuCAG3′tsRNA suppressed 5′ETS processing in 18S rRNA biogenesis in 293T and HCT-116 cells. Northern hybridization was performed with total RNA from HCT-116 and 293T cells 24 h post-transfection. The ITS1 probe detects the 45S primary transcript and intermediate forms of the mature 18S rRNA including 41S, 30S, 21S, and 18S-E pre-rRNAs. The 5′ETS probe detects the 45S primary transcript and 30S intermediate form of the mature 18S rRNA. Each number, multiplied by 10^4, on top of image represents the number of cells plated on 6-well culture dishes the day prior to transfection (n=2 independent experiments). For gel source data, see Supplementary Figure 1.

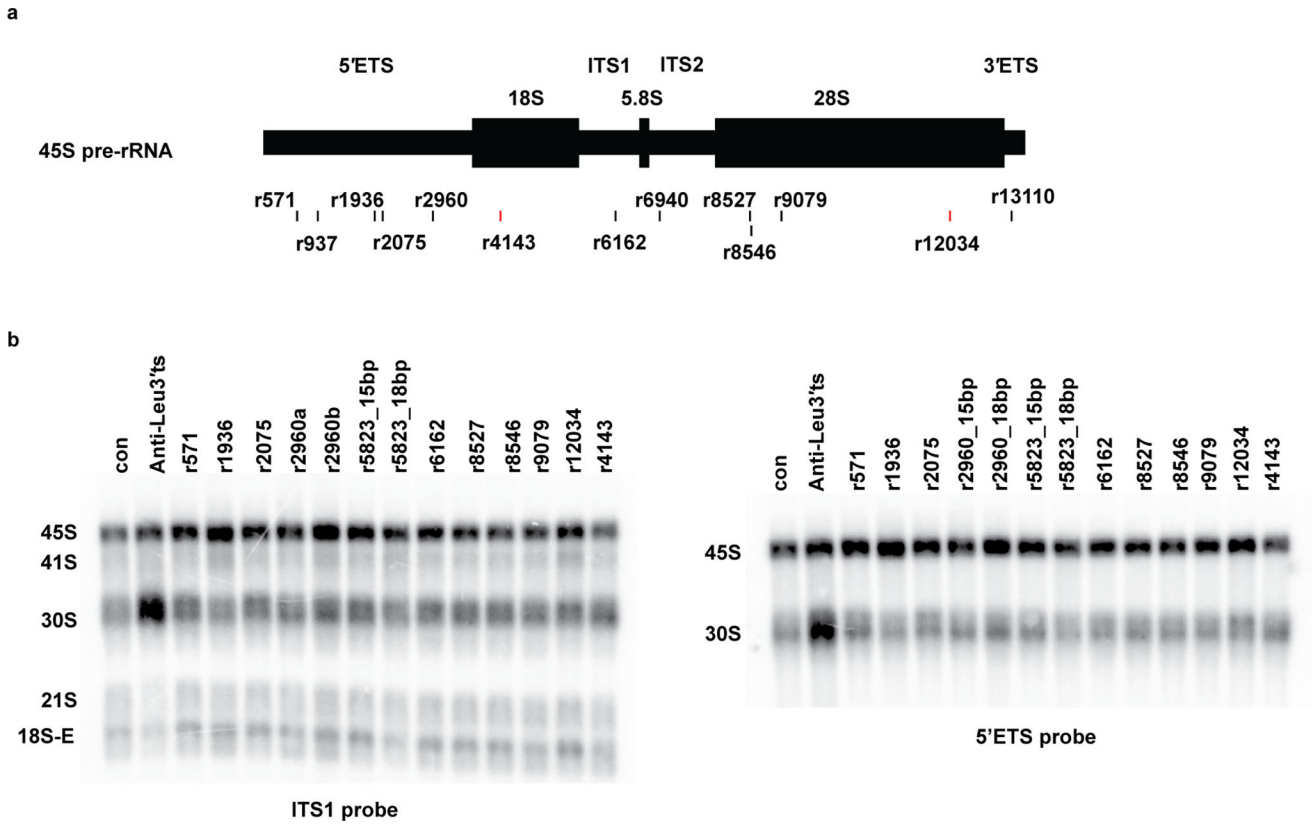

Extended Data Figure 5. LeuCAG3′tsRNA and anti-Leu3′tsLNA do not affect 18S rRNA biogenesis through binding to 45S pre-rRNA

a, Schematic picture showing putative binding sites of the LeuCAG3′tsRNA and anti-Leu3′tsLNA on the 45S primary transcript (45S pre-rRNA). To identify the tsRNA binding sites in the 45S pre-rRNA, we used the RNAhybrid program and 18- and 22-nt sequences from the 3′ end of LeuCAG-tRNA. The resulting five putative binding sites were positioned in the 5′ETS, 1 site in ITS1, 1 site in ITS2, 3 sites in 28S rRNA, and 1 site in the 3′ETS. The putative LeuCAG3′tsRNA binding site is indicated as a black bar. The putative binding site of anti-Leu3′tsLNA is indicated as a red bar. **b,** LeuCAG3′tsRNA and anti-Leu3′tsLNA do not bind to 45S pre-rRNA. To inhibit the interaction between LeuCAG3′tsRNA (or anti-

Leu3′tsLNA) and 45S pre-rRNA, each LNA design was based on the sequence shown in (**a**) and transfected into HeLa cells for 24 h prior to RNA extraction and northern hybridization (n=2 independent experiments). The sequences of each LNA are listed on Supplementary Table 4. For gel source data, see Supplementary Figure 1.

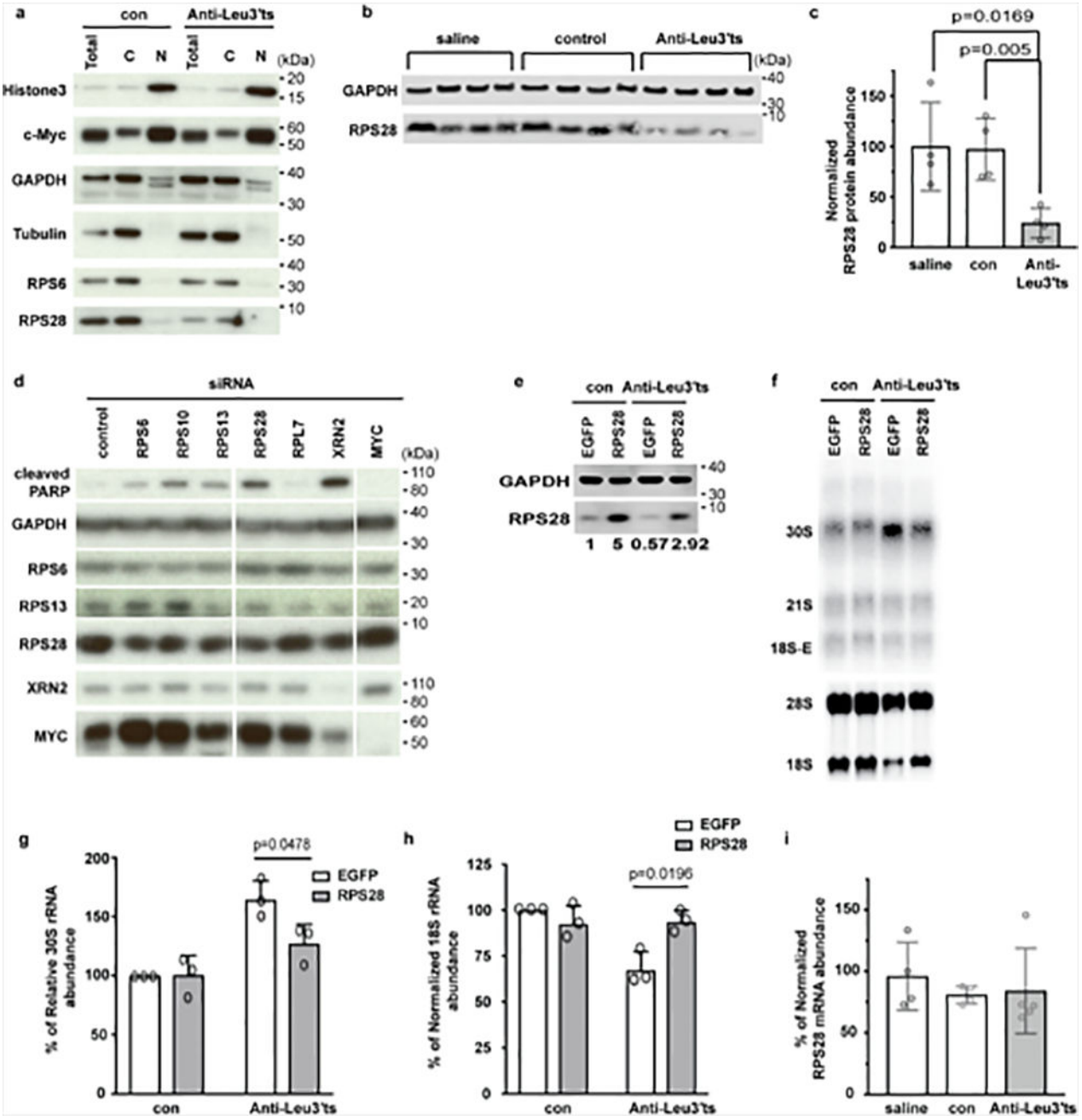

Extended Data Figure 6. Inhibition of LeuCAG3′tsRNA decreases RPS28 protein level, inducing apoptosis

a, Inhibition of the LeuCAG3'tsRNA does not change the nuclear-cytoplasmic subcellular localization of RPS6 and RPS28 proteins in HeLa cells. Western blotting was performed 24 h post transfection. (n=2 independent experiments). Total, total extracts; C, cytoplasm; N,

nucleus. **b and c,** RPS28 protein levels were down-regulated in anti-Leu3′tsLNA-treated HCC samples isolated from the orthotopic PDX. **b,** Total protein extracts from tumors (Extended Data Fig 2i) were subjected to western blotting (n=4 independent experiments). **c,** Quantification of the RPS28 protein level (n=4 independent experiments). **d,** A decrease in RPS28 protein level induces apoptosis in HeLa cells. Western blotting was performed 24 h post transfection of indicated siRNA (n=2 independent experiments). GAPDH, the loading control. **e,** RPS28 overexpression in HeLa cells for Fig. 4c and Extended Data Fig. 6e–h. The number below the image represents the relative RPS28 protein level normalized to GAPDH (n=2 independent experiments). **f–h,** Overexpression of RPS28 restores 18S rRNA processing. After co-transfection with the indicated LNAs and plasmids in HeLa cells for 24 h, northern blots using probes complementary to the 18S rRNA precursor, 18S and 28S rRNA as in (Fig. 3e) are shown. **f,** A representative northern result (n=3 independent experiments). **g,** Relative abundance of 30S pre-rRNA (n=3 independent experiments). **h,** Relative abundance of 18S rRNA normalized to 28S rRNA. Each value is normalized to that of con-EGFP transfected cells, which was set at 100 (n=3 independent experiments). **i,** RPS28 mRNA levels were unchanged in anti-Leu3′tsLNA treated HCC samples isolated from an orthotopic patient derived xenograft. RT- PCR was performed with total RNA from tumors (Fig. 2d). Each mRNA level was normalized to GAPDH mRNA (con and saline groups, n=4; Anti-Leu3′ts LNA group, n=5). Mean is indicated. Error bar, s.d.; indicated p-value by two-tailed t-test (c, g, h). For gel source data, see Supplementary Figure 1.

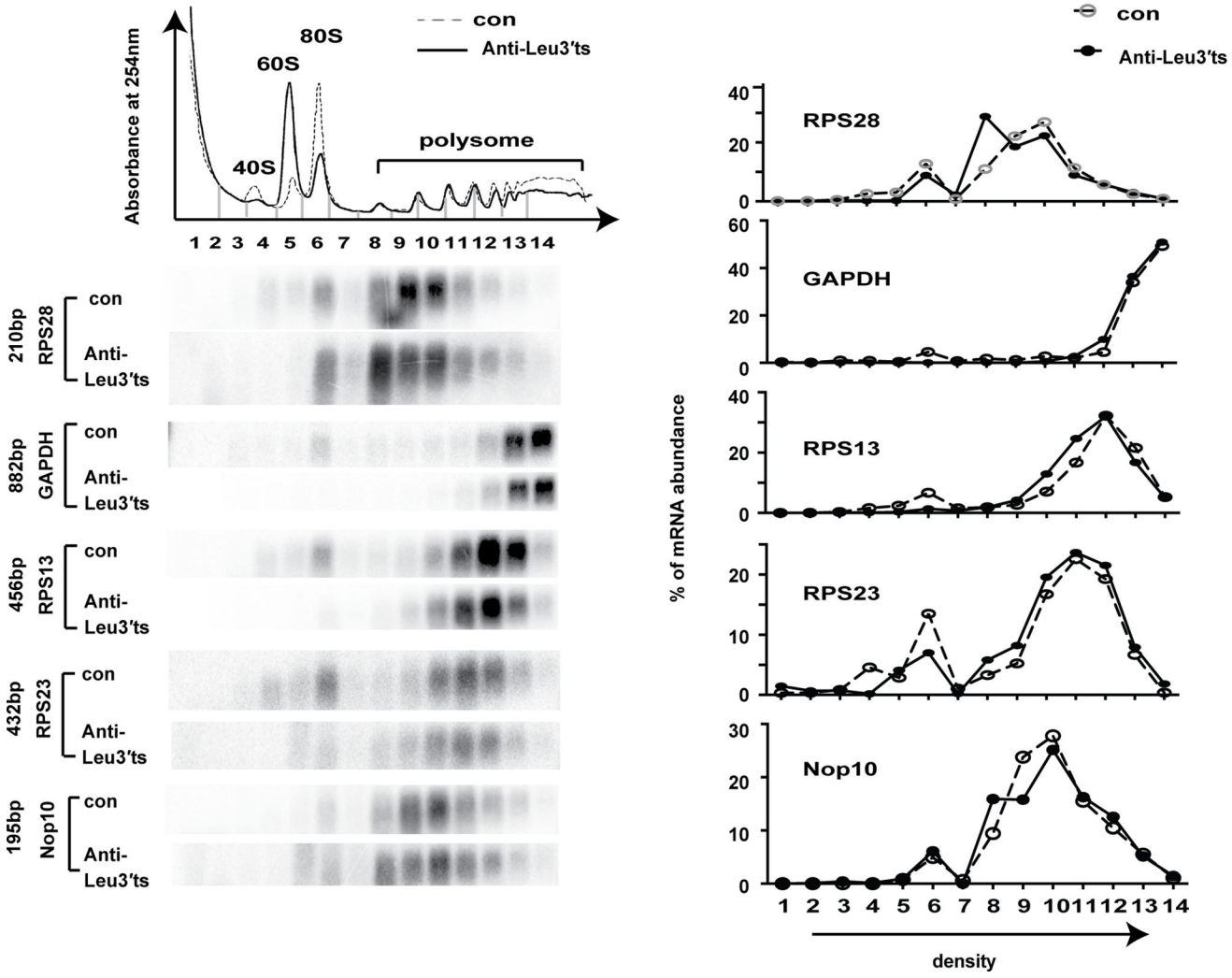

Extended Data Figure 7. Inhibition of LeuCAG3′tsRNA specifically alters sedimentation of RPS28 mRNA

Total RNA from each sucrose gradient fraction in Fig. 3a was extracted (left), and a northern analysis performed. The indicated bp provided to the left of the labeled gene name indicates the size of the coding sequences. The polysome profile is the same as shown in Fig. 3a. Relative distribution of mRNA populations across the gradient (right). Each amount of the specific mRNA for each gradient fraction was normalized using the sum of the mRNA signal across all gradient fractions. X-axis is the gradient fraction number; y-axis is % of mRNA abundance (n=2 independent experiments). For gel source data, see Supplementary Figure 1.

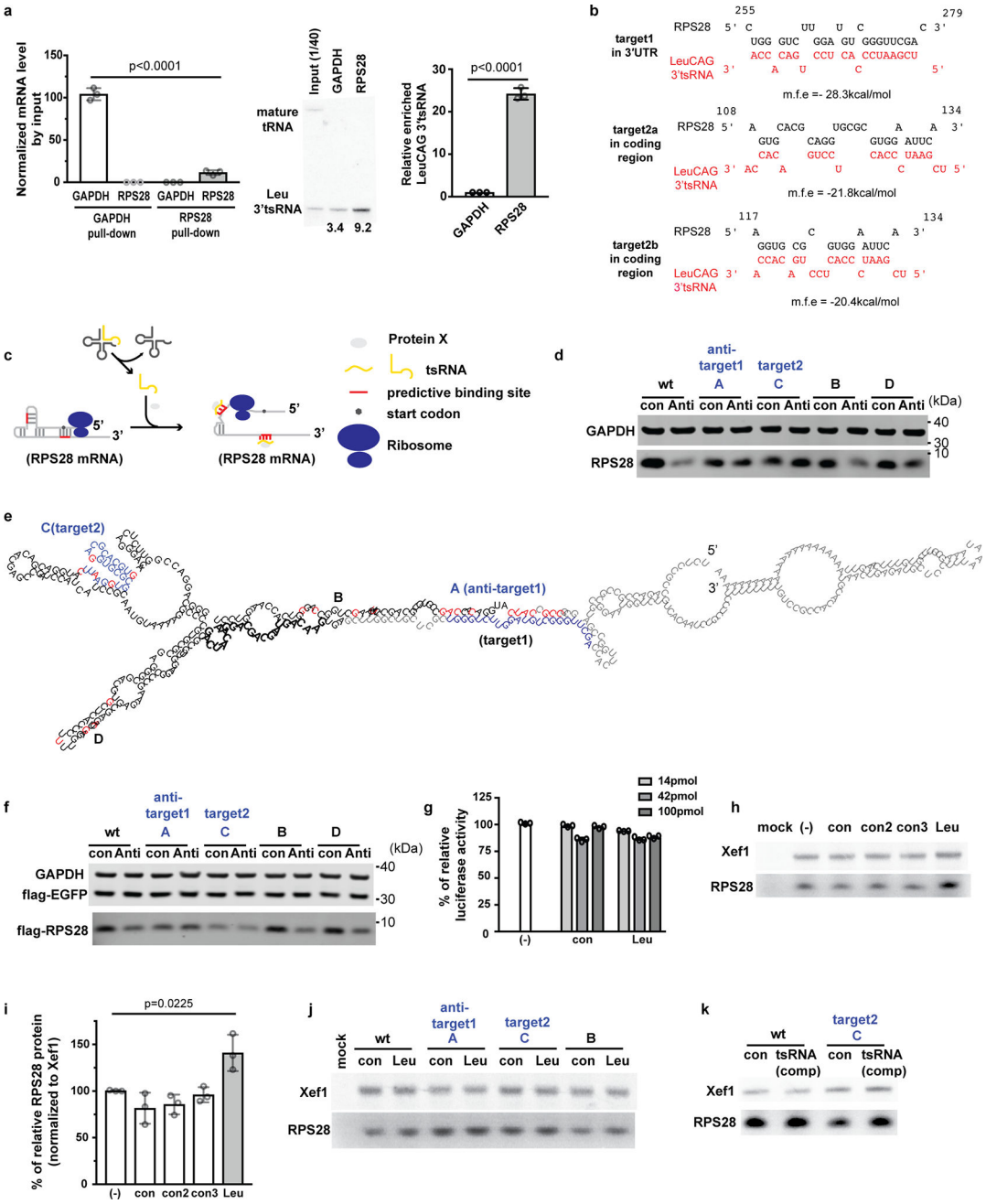

Extended Data Figure 8. LeuCAG3′tsRNA regulates RPS28 mRNA translation

a, LeuCAG3′tsRNA is associated with the RPS28 mRNA. *RPS28* or *GAPDH* mRNAs were pulled down with tiling oligos. The enrichment of each mRNA was measured by RT-PCR (left). The associated LeuCAG3′tsRNA was detected by northern hybridization (middle). The relative percentage of associated LeuCAG3′tsRNA is shown. The LeuCAG3′tsRNA was enriched 26-times (right) in the *RPS28* versus *GAPDH* mRNA pulldown after normalization (left). **b,** The two putative LeuCAG3′tsRNA binding sites in the *RPS28* mRNA. Target-site 1 (nt 255 to 279) in the 3′ UTR. Target-site 2 in the coding sequence (CDS) has two possible predicted configurations (target 2a (nt 108–134) and target2b (nt

117–134). The target2 mutant (labeled C in Fig. 5a and Extended Data Fig. 8e) alters both predicted target 2a and 2b conformations. **c**, Proposed model of translational regulation. The 3′tsRNA binds to the RPS28 mRNA and disrupts the secondary structure resulting in enhanced mRNA translation. Protein X, unknown protein(s). **d,** RPS28 protein levels are affected by the LeuCAG3′tsRNA concentration when the target sites remain unchanged. A representative western result after co-transfection of LNAs (con and Anti-Leu3′ts) and the RPS28 mutant plasmids. The relative RPS28 protein level was calculated after normalization to GAPDH (Fig. 5b). Con, control; Anti, anti-Leu3′tsLNA; wt, wild-type construct; other mutant constructs (Fig. 5a and Supplementary Table 8). **e,** Schematic of C-terminal flag-tagged RPS28 secondary structure with putative LeuCAG3′tsRNA binding sites. Red, the altered sequences in each mutant; blue, the putative LeuCAG3′tsRNA binding sites in the RPS28 mRNA; black and grey, the coding and non-protein coding sequences, respectively. Black bold, C-terminal flag tag sequences. **f,** The C-terminal flag-tagged RPS28 protein level is affected by LeuCAG3′tsRNA concentrations when the target sites remain unchanged. A representative western result after co-transfection of LNAs (con and Anti-Leu3′ts) and plasmids (flag-RPS28 and flag-EGFP). The relative RPS28 signal is shown in Fig. 5b and calculated after normalization to co-transfected flag tagged EGFP. **g**, Uncapped firefly luciferase mRNA was translated in rabbit reticulocyte lysate (RRL) with the indicated amounts of synthetic LeuCAG3′tsRNA (Leu). **h,** Synthetic LeuCAG3′tsRNA increases RPS28 mRNA translation *in vitro*. Xef1 (control) and RPS28 mRNAs were translated with a synthetic LeuCAG3′tsRNA *in vitro*. mock, no mRNA; (-), no control and LeuCAG3′tsRNA; con1, con2, and con3, three different control RNA. **i**, The relative RPS28 translation product was normalized to Xef1 from (**h**). **j**, Leu3′tsRNA does not affect translation of RPS28 *in vitro* when the putative binding sites are altered. Xef1 and RPS28 wt or mutant mRNAs were translated in RRL. The normalized RPS28 protein level is shown in Fig. 5c. **k,** RPS28 target2 mutant C translation was enhanced by a compensatory tsRNA mimic (tsRNA(comp)) nearly complementary to sequence-modified target2 site sequences from mutant C. Xef1 and RPS28 wt or mutant C mRNAs were translated with the compensatory tsRNA mimic (tsRNA(comp)). Normalized quantification of the RPS28 translation products is shown in Fig. 5d. Each western and IVT figure was cropped from a single image (gel source data, Supplementary Fig. 1). Mean is indicated. Error bar, s.d.; p-value by two-tailed t-test (a, i). For a,d,f,g-j (n=3) and k (n=4) independent experiments, respectively.

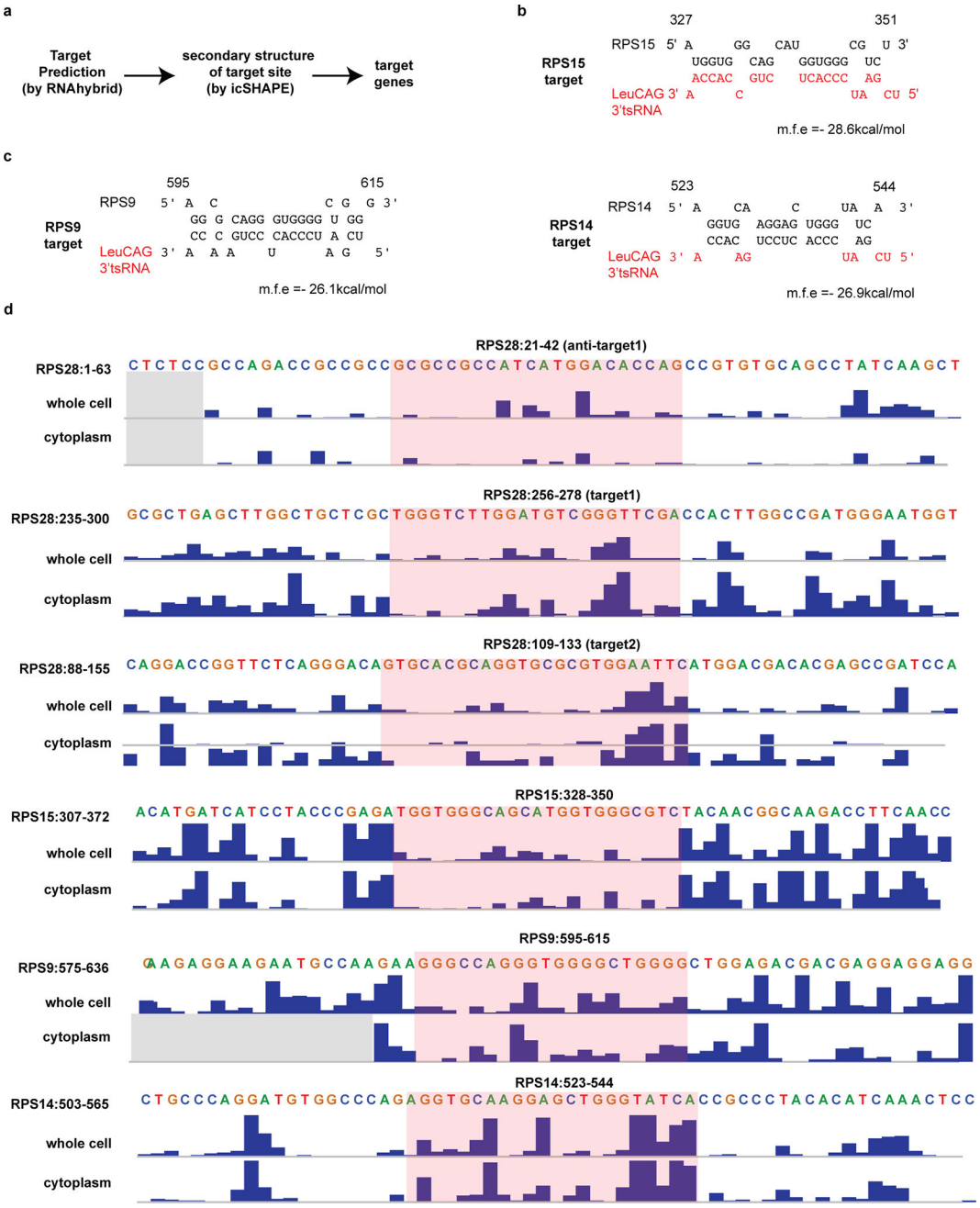

Extended Data Figure 9. Double-strandedness of LeuCAG3′tsRNA target sites

a, Schematic prediction of LeuCAG3′tsRNA binding sites. The target sites of the LeuCAG3′tsRNA in the coding sequences (CDSs) and flanking 30 bp of each mRNA were predicted using RNAhybrid based on the m.f.e. Secondary structures of target sites that were predicted to have a binding site based on the low m.f.e. were analyzed by icSHAPE. **b, c** Thermodynamics of the putative LeuCAG3′tsRNA binding sites in the RPS15 (**b**), RPS9 and RPS14 (**c**) mRNAs. Indicated numbers on each diagram represents the 5′ end and 3′ end position on each mRNA, respectively. **d,** The icSHAPE data track of LeuCAG3′tsRNA binding sites and 20 nt of flanking regions contained within the RPS28, RPS15, RPS9, and

RPS14 mRNAs. The icSHAPE data are scaled from 0 (no reactivity; double-strandedness) to 1 (maximum reactivity; single-strandedness). Red box represents a target site. The complete icSHAPE data for each mRNA are in Supplementary Table 10.

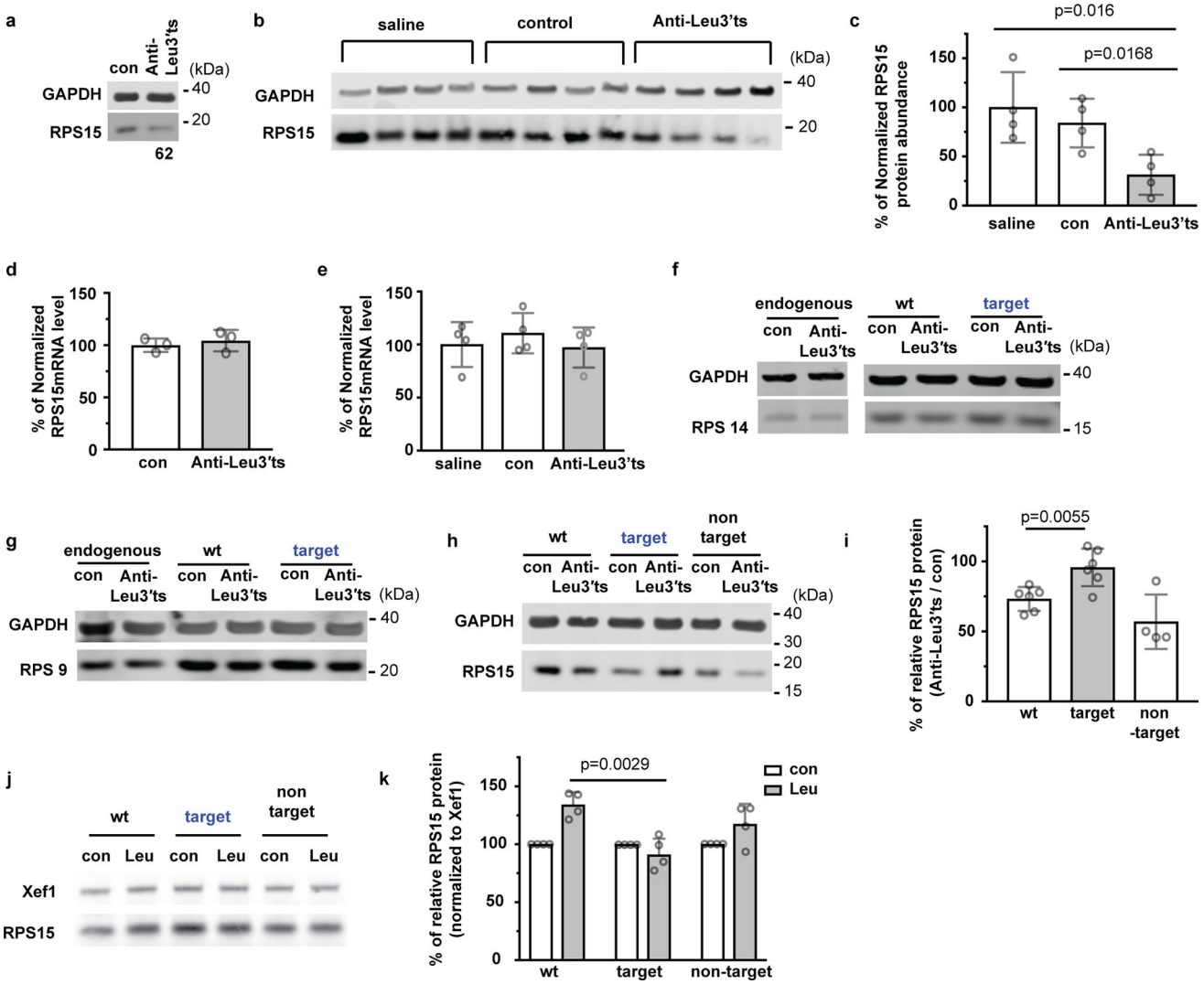

Extended Data Figure 10. The tsRNA affects RPS15 but not RPS9 and RPS14 protein levels

a, LeuCAG3′tsRNA inhibition decreases the RPS15 protein concentration. Protein levels were determined by western blot (n=3 independent experiments). The number under the image is the relative RPS15 protein level (anti-Leu3′tsLNA) normalized to control (con). **b,** RPS15 protein levels were down-regulated in anti-Leu3′tsLNA-treated HCC orthotopic PDX. Western blotting was performed with PDX tumors (Extended Data Fig 2i) (n=4 independent mice). **c,** Quantification of the RPS15 protein level from (**b**) (n=4 independent mice). **d**, Inhibition of LeuCAG3′tsRNA does not alter *RPS15* mRNA levels. RT-PCR was performed (n=3 independent experiments). **e,** *RPS15* mRNA levels were unchanged in anti-Leu3′tsLNA treated HCC orthotopic PDX. RT-PCR was performed with total RNA from tumors (Extended Data Fig. 2i) (n=4 independent mice). **f, g,** The RPS9 and RPS14 wt and target site mutant protein levels are not affected by LeuCAG3′tsRNA concentrations. A

representative western result after co-transfection of LNAs (con and Anti-Leu3′ts) and RPS9 wt or target mutant plasmids (f), and RPS14 wt or target mutant plasmids (g) (each n=2 independent experiments). Target, modified target site mutant. **h,** The RPS15 protein level is affected by LeuCAG3′tsRNA concentrations when the target site is not altered. Western blotting was performed as in (f) (n=4 independent experiments). Non target, modified non-target site mutant. **i,** The normalized RPS15 protein level from (**h**) was calculated as in Extended Data Fig. 8d (wt and target group, n=6; non-target group, n=4 independent experiments). **j,** Leu3′tsRNA does not affect translation of *RPS15* mRNA *in vitro* when the target site is altered. Xef1 and RPS15 wt or mutant mRNAs were translated in RRL as in Fig. 5c (n=4 independent experiments). **k,** The normalized RPS15 protein level from (**j**) (n=4 independent experiments). Each gel figure was cropped from a single image. Normalization of RT-PCR result is described in the Methods. Mean is indicated. Error bar, s.d.; indicated p-value by two-tailed t-test (**c, i, k**). For gel source data, see Supplementary Figure 1. The mutant constructs are listed in Supplementary Table 8.

Supplementary Material

Refer to Web version on PubMed Central for supplementary material.

Acknowledgments

We thank J. Sage (Stanford University) for HCC tissues from conditional TKO ($Rb^{lox/lox}$; $p130^{lox/lox}$; $p107^{-/-}$) adult mice and liver tissues from $p107^{-/-}$ mice. This work was supported by grants to M.A.K. from the National Institutes of Health (R01AI071068 and R01DK114483). M.A.K. received support from the Stanford Cancer Institute, and S.S. from the CJ Huang Foundation and the TS Kwok Liver Cancer Foundation.

References

1. Gebetsberger J, Polacek N. Slicing tRNAs to boost functional ncRNA diversity. RNA Biology. 2013; 10:1798–1806. [PubMed: 24351723]
2. Thompson DM, Parker R. Stressing out over tRNA cleavage. 2009; 138:215–219.
3. Yamasaki S, Ivanov P, Hu G-F, Anderson P. Angiogenin cleaves tRNA and promotes stress-induced translational repression. The Journal of Cell Biology. 2009; 185:35–42. [PubMed: 19332886]
4. Honda S, et al. Sex hormone-dependent tRNA halves enhance cell proliferation in breast and prostate cancers. Proc Natl Acad Sci USA. 2015; doi: 10.1073/pnas.1510077112
5. Chen Q, et al. Sperm tsRNAs contribute to intergenerational inheritance of an acquired metabolic disorder. Science. 2016; 351:397–400. [PubMed: 26721680]
6. Sharma U, et al. Biogenesis and function of tRNA fragments during sperm maturation and fertilization in mammals. Science. 2016; 351:391–396. [PubMed: 26721685]
7. Kumar P, Kuscu C, Dutta A. Biogenesis and Function of Transfer RNA-Related Fragments (tRFs). Trends Biochem Sci. 2016; 41:679–689. [PubMed: 27263052]
8. Blanco S, et al. Stem cell function and stress response are controlled by protein synthesis. Nature. 2016; 534:335–340. [PubMed: 27306184]
9. Ivanov P, Emara MM, Villen J, Gygi SP, Anderson P. Angiogenin-induced tRNA fragments inhibit translation initiation. Mol Cell. 2011; 43:613–623. [PubMed: 21855800]
10. Schorn AJ, Gutbrod MJ, LeBlanc C, Martienssen R. LTR-Retrotransposon Control by tRNA-Derived Small RNAs. Cell. 2017; 170:61–71.e11. [PubMed: 28666125]
11. Martinez G, Choudury SG, Slotkin RK. tRNA-derived small RNAs target transposable element transcripts. Nucleic Acids Res. 2017; doi: 10.1093/nar/gkx103
12. Haussecker D, et al. Human tRNA-derived small RNAs in the global regulation of RNA silencing. RNA. 2010; 16:673–695. [PubMed: 20181738]

13. Maute RL, et al. tRNA-derived microRNA modulates proliferation and the DNA damage response and is down-regulated in B cell lymphoma. Proc Natl Acad Sci USA. 2013; 110:1404–1409. [PubMed: 23297232]
14. Kumar P, Anaya J, Mudunuri SB, Dutta A. Meta-analysis of tRNA derived RNA fragments reveals that they are evolutionarily conserved and associate with AGO proteins to recognize specific RNA targets. BMC Biol. 2014; 12:78. [PubMed: 25270025]
15. Jepsen JS, Sørensen MD, Wengel J. Locked nucleic acid: a potent nucleic acid analog in therapeutics and biotechnology. Oligonucleotides. 2004; 14:130–146. [PubMed: 15294076]
16. Elmén J, et al. LNA-mediated microRNA silencing in non-human primates. Nature. 2008; 452:896–899. [PubMed: 18368051]
17. Berridge MV, Herst PM, Tan AS. Tetrazolium dyes as tools in cell biology: new insights into their cellular reduction. Biotechnol Annu Rev. 2005; 11:127–152. [PubMed: 16216776]
18. Cozen AE, et al. ARM-seq: AlkB-facilitated RNA methylation sequencing reveals a complex landscape of modified tRNA fragments. Nat Meth. 2015; 12:879–884.
19. Zheng G, et al. Efficient and quantitative high-throughput tRNA sequencing. Nat Meth. 2015; 12:835–837.
20. Elmore S. Apoptosis: a review of programmed cell death. Toxicol Pathol. 2007; 35:495–516. [PubMed: 17562483]
21. Blobel G, Sabatini D. Dissociation of Mammalian Polyribosomes Into Subunits by Puromycin. Proc Natl Acad Sci USA. 1971; 68:390–394. [PubMed: 5277091]
22. Robledo S, et al. The role of human ribosomal proteins in the maturation of rRNA and ribosome production. RNA. 2008; 14:1918–1929. [PubMed: 18697920]
23. Oskarsson T, Trumpp A. The Myc trilogy: lord of RNA polymerases. Nat. Cell Biol. 2005; 7:215–217. [PubMed: 15738972]
24. Dianzani I, Loreni F. Diamond-Blackfan anemia: a ribosomal puzzle. Haematologica. 2008; 93:1601–1604. [PubMed: 18978295]
25. Donati G, Montanaro L, Derenzini M. Ribosome biogenesis and control of cell proliferation: p53 is not alone. Cancer Res. 2012; 72:1602–1607. [PubMed: 22282659]
26. Chu C, Quinn J, Chang HY. Chromatin isolation by RNA purification (ChIRP). J Vis Exp. 2012; doi: 10.3791/3912
27. Roy-Chaudhuri B, et al. Regulation of microRNA-mediated gene silencing by microRNA precursors. Nature Structural & Molecular Biology. 2014; 21:825–832.
28. Rehmsmeier M, Steffen P, Hochsmann M, Giegerich R. Fast and effective prediction of microRNA/target duplexes. RNA. 2004; 10:1507–1517. [PubMed: 15383676]
29. Hofacker IL, Stadler PF. Memory efficient folding algorithms for circular RNA secondary structures. Bioinformatics. 2006; 22:1172–1176. [PubMed: 16452114]
30. Zuker M. Mfold web server for nucleic acid folding and hybridization prediction. Nucleic Acids Res. 2003; 31:3406–3415. [PubMed: 12824337]
31. Reuter JS, Mathews DH. RNAstructure: software for RNA secondary structure prediction and analysis. BMC Bioinformatics. 2010; 11:129. [PubMed: 20230624]
32. Yan K, et al. Structure Prediction: New Insights into Decrypting Long Noncoding RNAs. Int J Mol Sci. 2016; 17:132.
33. Lu Z, et al. RNA Duplex Map in Living Cells Reveals Higher-Order Transcriptome Structure. 2016; 165:1267–1279.
34. Janas MM, et al. Reduced expression of ribosomal proteins relieves microRNA-mediated repression. Mol Cell. 2012; 46:171–186. [PubMed: 22541556]
35. Volarevic S, et al. Proliferation, but not growth, blocked by conditional deletion of 40S ribosomal protein S6. Science. 2000; 288:2045–2047. [PubMed: 10856218]
36. Wei W, et al. Novel celastrol derivatives inhibit the growth of hepatocellular carcinoma patient-derived xenografts. Oncotarget. 2014; 5:5819–5831. [PubMed: 25051375]
37. Liu F, Song Y, Liu D. Hydrodynamics-based transfection in animals by systemic administration of plasmid DNA. Gene Ther. 1999; 6:1258–1266. [PubMed: 10455434]

38. Zhang G, Budker V, Wolff JA. High levels of foreign gene expression in hepatocytes after tail vein injections of naked plasmid DNA. Hum. Gene Ther. 1999; 10:1735–1737. [PubMed: 10428218]
39. Trapnell C, Pachter L, Salzberg SL. TopHat: discovering splice junctions with RNA-Seq. Bioinformatics. 2009; 25:1105–1111. [PubMed: 19289445]
40. Trapnell C, et al. Transcript assembly and quantification by RNA-Seq reveals unannotated transcripts and isoform switching during cell differentiation. Nat Biotechnol. 2010; 28:511–515. [PubMed: 20436464]
41. Trapnell C, et al. Differential gene and transcript expression analysis of RNA-seq experiments with TopHat and Cufflinks. Nat Protoc. 2012; 7:562–578. [PubMed: 22383036]
42. Fuchs G, Diges C, Kohlstaedt LA, Wehner KA, Sarnow P. Proteomic analysis of ribosomes: translational control of mRNA populations by glycogen synthase GYS1. J. Mol. Biol. 2011; 410:118–130. [PubMed: 21570405]
43. Viatour P, et al. Hematopoietic stem cell quiescence is maintained by compound contributions of the retinoblastoma gene family. Cell Stem Cell. 2008; 3:416–428. [PubMed: 18940733]
44. Hasler D, et al. The Lupus Autoantigen La Prevents Mis-channeling of tRNA Fragments into the Human MicroRNA Pathway. Mol Cell. 2016; 63:110–124. [PubMed: 27345152]
45. Hadjiolova KV, Nicoloso M, Mazan S, Hadjiolov AA, Bachellerie JP. Alternative pre-rRNA processing pathways in human cells and their alteration by cycloheximide inhibition of protein synthesis. Eur. J. Biochem. 1993; 212:211–215. [PubMed: 8444156]
46. Choesmel V, et al. Mutation of ribosomal protein RPS24 in Diamond-Blackfan anemia results in a ribosome biogenesis disorder. Hum. Mol. Genet. 2008; 17:1253–1263. [PubMed: 18230666]

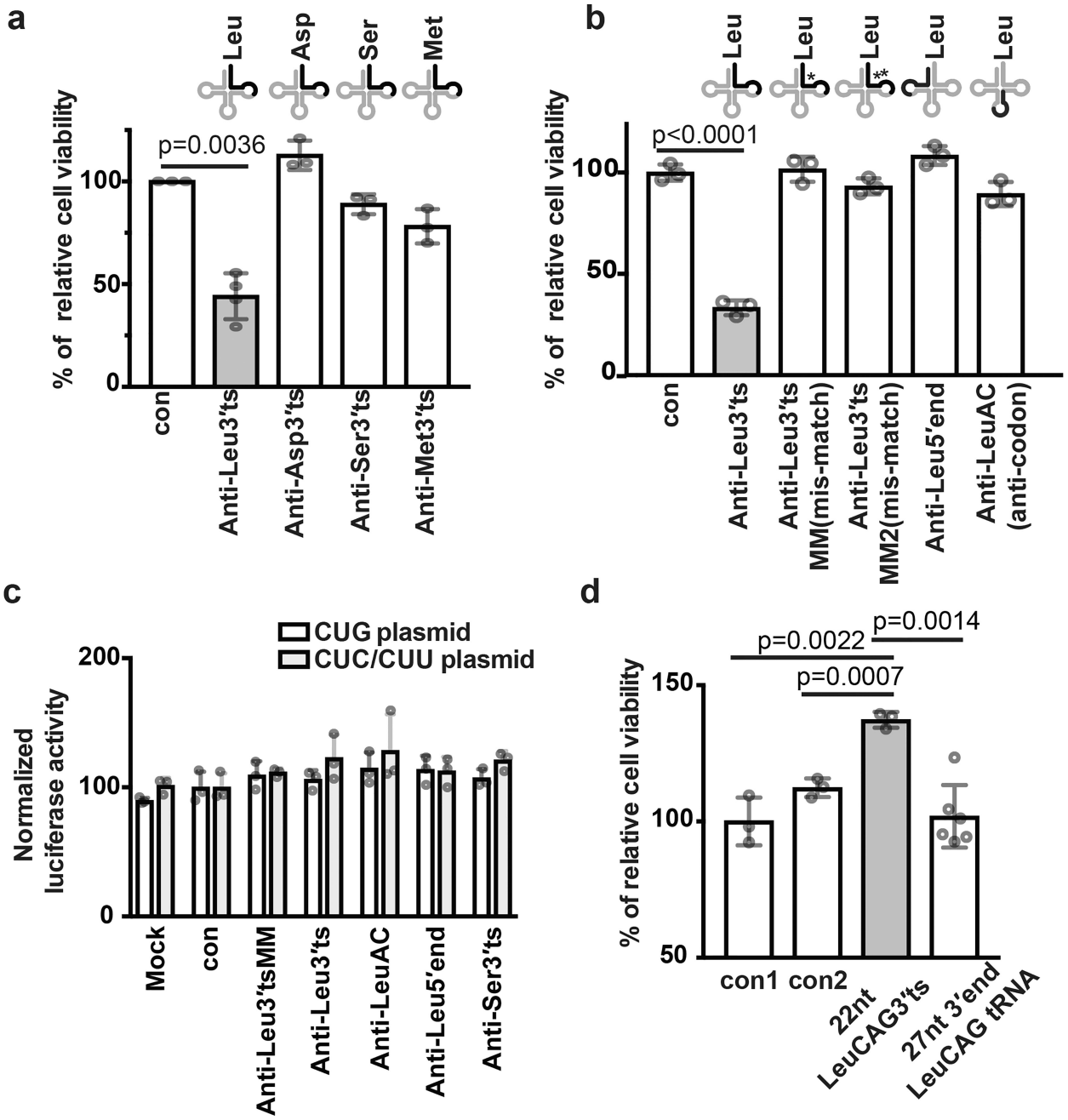

Figure 1. LeuCAG3′tsRNA is required for cell viability

a, b, Inhibition of the LeuCAG3′tsRNA impairs HeLa cell viability. 3 days post-transfection, a MTS assay was performed (Anti-Leu3′ts(LNA), n=4; others, n=3 independent experiments). The indicated mixmer LNA is perfectly complementary to the darkened portion of the tRNA above the bar graph. Different asterisk marks in (**b**) depict different 2-nt mismatches; con, control mixmer LNA. **c,** Inhibition of the LeuCAG3′tsRNA does not affect the function of the mature LeuCAG-tRNA. A Luciferase assay was performed 24 h after co-transfection of the designated LNA and luciferase plasmid. The CUG plasmid has the unmodified *Renilla* and firefly luciferase gene. The CUC/CUU

plasmid contains unmodified firefly and modified *Renilla* gene where 13 CUG codons were replaced with CUC or CUU codons (n=3 independent experiments) (Supplementary Table 1). Normalization is described in the Methods. **d,** The 22-nt synthetic LeuCAG3′tsRNA enhances cell viability. The MTS assay was performed as in (a) (27-nt 3′ end of LeuCAG-tRNA, n=6; others, n=3 independent experiments). Con1 and con2, different scrambled sequences; 22-nt LeuCAG3′tsRNA and 27-nt 3′ end of LeuCAG-tRNA sequences, 22- and 27-nt sequences from the 3′ end of mature LeuCAG-tRNA. Mean is indicated. Error bar, s.d.; indicated p-value by two-tailed t-test (a, b, c, d).

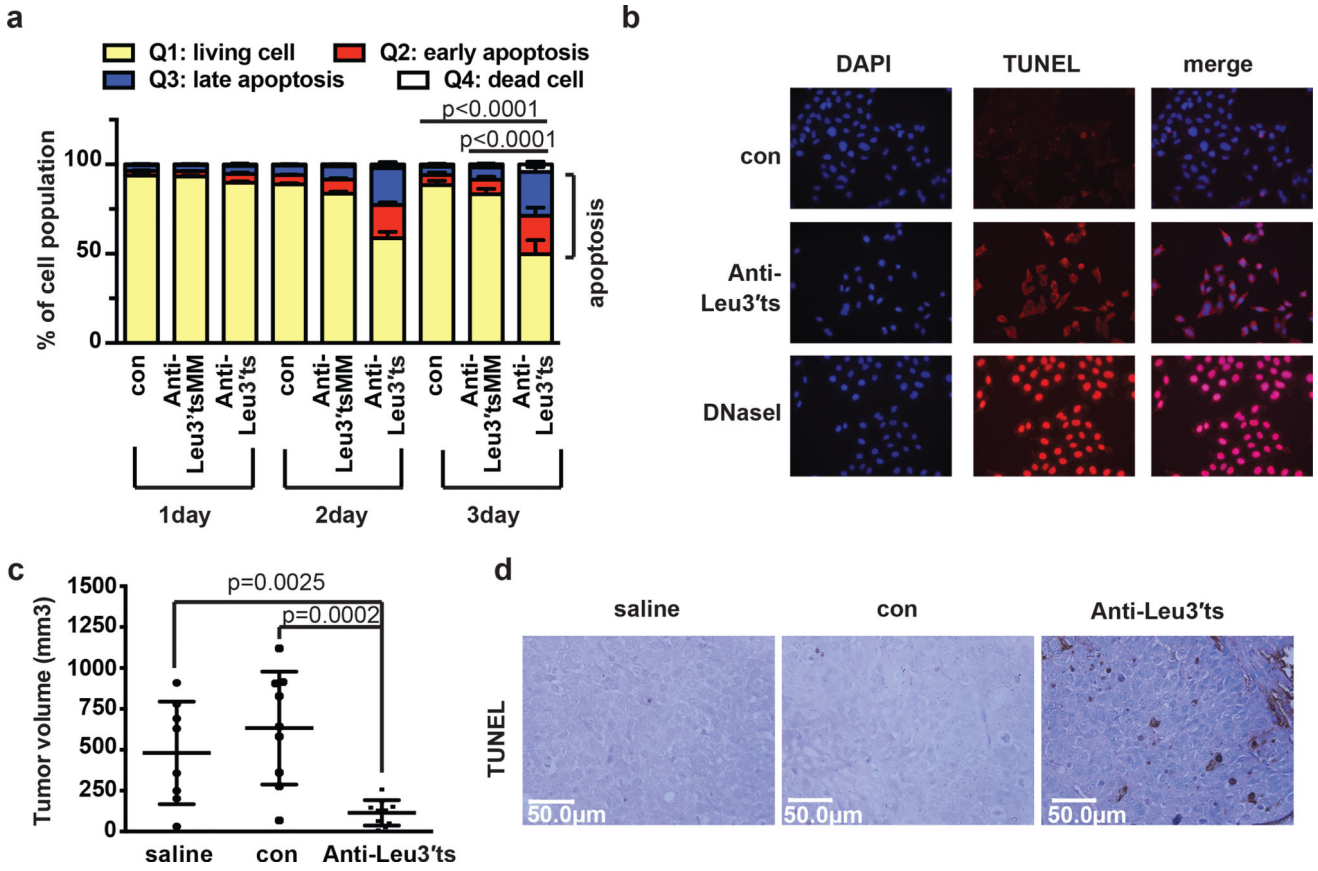

Figure 2. Inhibition of LeuCAG3′tsRNA induces apoptosis and inhibits the growth of hepatocellular carcinoma (HCC) patient-derived xenograft

a, Apoptotic HeLa cell populations were determined using Annexin V-FITC and PI staining every 24 h post-transfection (each at 1 day, n=3; Anti-Leu3′tsLNA at 3 day, n=5; others, n=4 biological replicates) (Extended Data Fig. 2a). **b,** TUNEL assay in HeLa cells, 24 h post transfection (n=2 independent experiments). DNase I, positive control. DAPI staining, nuclei. **c,** Patient-derived orthotopic HCC tumor volume. Administration of the Anti-Leu3′tsLNA or control materials (saline or con LNA) were performed by IP injections. After the 4-week injection period, all mice were sacrificed and tumors harvested (Extended Data Fig. 2i) and measured (saline, n=8; con, n=9; Anti-Leu3′ts, n=10 independent tumors). **d,** Representative TUNEL assay. Apoptotic cells are stained with a brown-colored nucleus (n=2 independent experiments). Mean is indicated. Error bar, s.d.; indicated p-value by two-tailed t-test (a, d); p-value (a), apoptosis population.

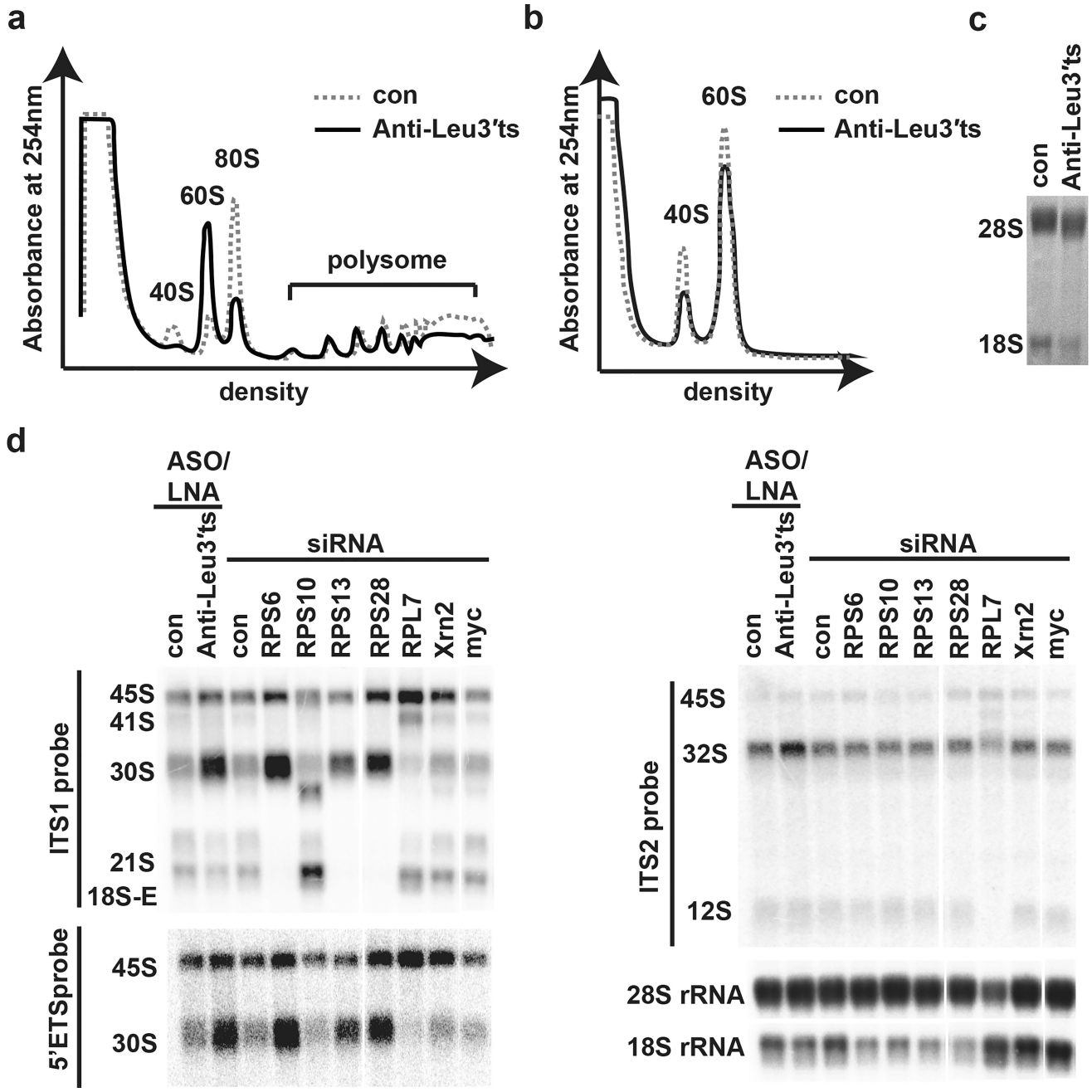

Figure 3. LeuCAG3′tsRNA is required for ribosome biogenesis

a, b, Inhibition of LeuCAG3′tsRNA decreases the amount of 40S ribosomal subunits. (**a**) Polysome profiles (n=3 independent experiments). (**b**) Ribosomal subunit profiles after puromycin-mediated dissociation (n=3 independent experiments). **c,** Inhibition of LeuCAG3′tsRNA decreases steady-state levels of 18S rRNA. Northern hybridization was performed in HeLa cells 24 h post-transfection (n=3 independent experiments). **d,** Inhibition of LeuCAG3′tsRNA suppressed removal of 5′ETS during 18S rRNA biogenesis. Northern hybridization was performed as in (**c**). Intermediate forms of mature 18S rRNA (30S, 21S, and 18S-E pre-rRNA) and mature 28S and 5.8S rRNAs (32S and 12S) were detected by the

ITS1 and ITS2 probes, respectively. 30S pre-rRNA is also detected by the 5′ETS1 probe (n=3 independent experiments). The rRNA processing pathway is described in Extended Data Fig. 4b. Each normalized pre-rRNA level is in Supplementary Table 3. For gel source data, see Supplementary Figure 1.

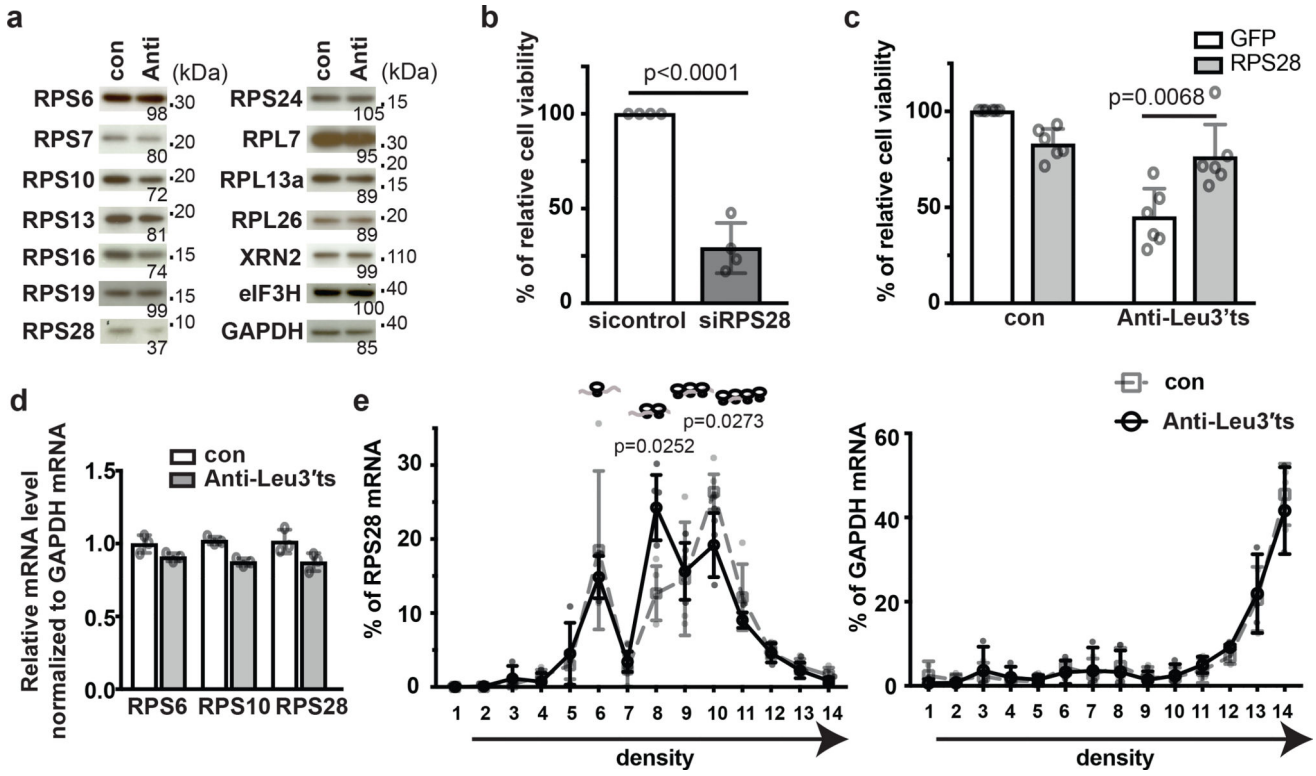

Figure 4. Inhibition of LeuCAG3′tsRNA down-regulates RPS28 mRNA translation

a, Western blotting of RPs from LeuCAG3′tsRNA-inhibited HeLa cells (n=3 independent experiments). GAPDH, loading control. The number below each image, relative protein level from Anti-Leu3′tsLNA-treated cells normalized to control. Con, control; Anti, Anti-Leu3′tsLNA. **b,** Decreased RPS28 protein concentrations impair HeLa cell viability, determined as in Fig. 1a (n=4 independent experiments). **c,** Overexpression of RPS28 protein increases cell viability. After co-transfection of the designated LNA and plasmids, cell viability was determined (n=6 independent experiments). **d,** Inhibition of LeuCAG3′tsRNA does not alter *RPS28* mRNA levels, determined by RT-PCR (n=3 independent experiments). **e,** Inhibition of LeuCAG3′tsRNA alters sedimentation of the RPS28 mRNA within the sucrose gradient. Northern analysis was performed on each gradient fraction. The amount of the specific mRNA for each fraction was normalized to the sum of the mRNA signal across all gradient fractions (RPS28, n=4; GAPDH, n=3 independent experiments). X-axis, fraction number. The diagram above each fraction, the number of ribosomes associated with mRNA based on a gradient profile (Fig. 3a). Mean is indicated. Error bar, s.d.; indicated p-value by two-tailed t-test (b–e). For gel source data, see Supplementary Figure 1.

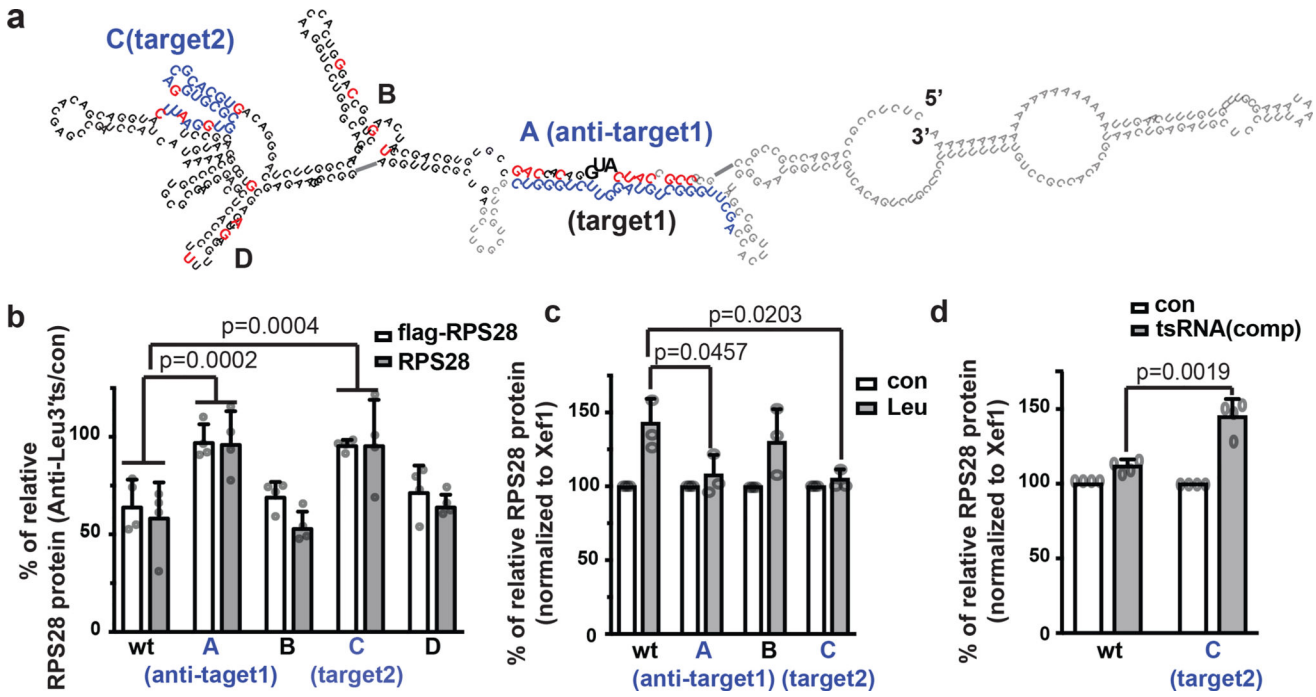

Figure 5. LeuCAG3′tsRNA is required for efficient translation of RPS28 through base-pairing with its mRNA

a, Schematic of the RPS28 mRNA secondary structure predicted by RNAfold. Red, modified nucleotide. Blue, potential binding sites of the LeuCAG3′tsRNA (Extended Data Fig. 8b). Black and grey, coding and untranslated sequences, respectively. **b,** A potential binding site is required for the tsRNA to regulate RPS28 protein production. The relative protein levels were determined as described in Extended Data Fig. 8d,f (n=4 independent experiments). X-axis indicates the RPS28 construct (Fig. 5a, Extended Data Fig. 8e and Supplementary Table 8). **c,** The Leu3′tsRNA does not affect translation of RPS28 mRNA *in vitro* when the potential binding sites are modified. Xef1 and RPS28 wt or mutant mRNAs were translated in RRL (Extended Data Fig. 8j) (n=3 independent experiments). (-), absence of control and LeuCAG3′tsRNA. **d,** RPS28 target2 mutant C translation was enhanced by a compensatory tsRNA mimic (tsRNA(comp)) complementary to the altered target2 sequence. *In vitro* translation was performed as in (c) (Extended Data Fig. 8k) (n=4 independent experiments). Relative *in vitro* translated RPS28 level was normalized to the Xef1 level (c, d). Mean is indicated. Error bar, s.d.; indicated p-value by two-tailed t-test (b–d).